Spring 4-22-2021

# PRECLINICAL DEVELOPMENT OF SINGLE WALLED CARBON NANOTUBE-BASED OPTICAL BIOSENSORS

Eric M. Hofferber
*University of Nebraska - Lincoln*, eric.hofferber@huskers.unl.edu

# PRECLINICAL DEVELOPMENT OF SINGLE WALLED CARBON NANOTUBE-BASED OPTICAL BIOSENSORS

by

Eric M. Hofferber

A DISSERTATION

Presented to the Faculty of

The Graduate College at the University of Nebraska

In Partial Fulfillment of Requirements

For the Degree of Doctor of Philosophy

Major: Biological Engineering

Under the Supervision of Professor Nicole M. Iverson

Lincoln, Nebraska

April, 2021

# PRECLINICAL DEVELOPMENT OF SINGLE WALLED CARBON NANOTUBE-BASED OPTICAL BIOSENSORS

Eric M. Hofferber, Ph.D.

University of Nebraska, 2021

Advisor: Nicole M. Iverson

High resolution, long-term monitoring of key biological analytes would improve patient outcomes by providing earlier detection of disease states and improved efficacy of treatment. One class of biosensors that have gained much attention in recent years are optical biosensors. Optical probes are attractive biosensors due to their noninvasive nature of detection, as certain light can pass through tissue, water, and blood. Single walled carbon nanotubes (SWNT) are a specific type of optical biosensor that fluoresce in the near infrared range of the electromagnetic spectrum and offer unparalleled spatial and temporal resolution. SWNT have been applied as biosensors *in vitro*, *ex vivo*, and *in vivo* for a growing library of key biological analytes. However, biocompatibility concerns, complex detection schemes, and platform incorporation have hindered translation of this promising class of biosensor to the clinical setting. Herein, novel characterization methods to determine SWNT fate, a simple detection scheme demonstrating the first successful detection of SWNT sensors in a large animal model, and novel platforms for localization of real time SWNT sensors are described. As a hydrophobic nanoparticle made of pure carbon, biocompatibility concerns persist when SWNT are used for biological applications. Following application *in vivo*, novel methods were developed to extract and quantify SWNT sensors accounting for the majority of the initial implant, and subsequent Raman spectroscopy measurements on excised tissue

resulted in no detectable SWNT aggregation. Nanotechnology laboratories are not well suited for large animal housing or handling, and detection schemes for SWNT are typically complex and immobile. To this end, a simple detection scheme of a noncoherent light source and a near-infrared spectrometer was applied to show successful detection of a SWNT fluorescence signal in a large animal for the first time. Finally, SWNT incorporation into platforms for localization have led to delayed or attenuated responses to the target analyte in the past. SWNT-hydrogel platforms were developed to investigate the underlying mechanisms for the delayed response, and platforms were developed that offered SWNT localization with negligible effect on sensitivity.

**ACKNOWLEDGEMENTS**

To my advisor Dr. Nicole Iverson, you forever changed my life five years ago when you gave me the wonderful opportunity to alter my path and allowed me to pursue something that I sincerely loved doing. When many others would not have given me the chance to return to school, you saw something in me. Your passion for research is undeniable and, with your guidance, knowledge, and understanding, has led me to become the researcher that I am today. You are truly a fantastic advisor and I am lucky to have had you as a mentor.

To my committee members, Dr. Greg Bashford, Dr. Forrest Kievit, and Dr. Yongfeng Lu, thank you for sharing your insights and genuine curiosity. I have been privileged to take courses with all of you along my journey that reminded me why I continued my education. I have also been truly fortunate to have had discussions with all of you that have not only helped shaped my research but have demonstrated that the enthusiasm for research and learning can be lifelong.

To my lab mates past and present, the friendships I have built with you have been essential to my success in graduate school. You have assisted me with experiments at all hours of the day or night, had lengthy discussions about crucial concepts, and been a support for me to lean on during difficult and hectic times.

To my wife Madeleine, I could not have done this without you. You have been with me since before this journey ever began, and your initial encouragement convinced me this was something that I could achieve. If it were not for the unwavering support and love you have given me throughout this journey, I would not be here today. Not only have your words motivated, but your hard work and determination in your own pursuits

have served as a constant reminder of what is possible. You never quit, even in the face of an impossibly difficult situation, you remained strong and graceful. I love you more than you could ever know.

To my brother and sister, Matt and Amanda, you both have always been there for me no matter how far apart we are or how busy our lives have become. You both have shown grit and perseverance in your own lives that has been a shining example to me on days that I did not think I could complete this work. I love you both.

Finally, to my parents, I will forever be grateful for the wonderful life you have given me. You instilled values in me that have made navigating life and its challenges infinitely easier. From your words and examples, I learned to work diligently, endure against all odds, and succeed with humility. However, the most important thing I learned from you was how to love unconditionally as you both have for your family and each other. I love you both.

# PREFACE

Chapter 2 is published: Hofferber E, Meier J, Herrera N, Stapleton J, Ney K, Francis B, Calkins C, Iverson NM. Novel Methods to Extract and Quantify Sensors based on Single Wall Carbon Nanotube Fluorescence from Animal Tissue and Hydrogel-Based Platforms. Methods Appl Fluoresc. 2021 Feb 25. Used with permission.

Chapter 3 is under review: Hofferber E, Meier J, Herrera N, Stapleton J, Calkins C, Iverson NM. Detection of Single Walled Carbon Nanotube Based Sensors in a Large Mammal. Submitted to Nanomedicine: NBM.

Chapter 4 is published: Hofferber, E. M., Stapleton, J. A., Adams, J., Kuss, M., Duan, B., Iverson, N. M., Implantable Nanotube Sensor Platform for Rapid Analyte Detection. Macromol. Biosci. 2019, 19, 1800469. Used with permission.

# LIST OF ABBREVIATIONS

| | |
|---|---|
| AC | Alginate composite |
| ALC | Alginate liquid-core |
| ATPES | 3-aminopropyltriethoxysilane |
| BSA | Bovine serum albumin |
| CNT | Carbon nanotube |
| $d(AT)_{15}$ | Oligonucleotide (adenine thymine repeated 15 times) |
| DNA | Deoxyribonucleic acid |
| FF SWNT | Free floating SWNT |
| FWHM | Full width half max |
| GFP | Green fluorescent protein |
| $H_2O_2$ | Hydrogen peroxide |
| HA | Hyaluronic acid |
| HALC | Hyaluronic acid liquid-core |
| HE4 | Human epididymis protein 4 |
| HiPco | High-pressure carbon monoxide |
| HIV | Human immunodeficiency virus |
| HOMO | Highest occupied molecular orbit |
| HRP | Horseradish peroxidase |
| HUVEC | Human umbilical vein endothelial cells |
| IgD | Human immunoglobin D |
| IgG | Human immunoglobin G |

| | |
|---|---|
| InGaAs | Indium gallium arsenide |
| IR | Infrared |
| LDL | Low-density lipoproteins |
| LED | Light-emitting diode |
| LUMO | Lowest unoccupied molecular orbit |
| MWNT | Multi walled carbon nanotube |
| nIR | Near infrared |
| NO | Nitric oxide |
| NOS | Nitric oxide synthase |
| PBS | Phosphate-buffered saline |
| PCD | Polycarbodiimide |
| PEG | Polyethylene glycol |
| PVP | Poly(vinylpyrrolidone) |
| RAP-1 | Ras-associated protein-1 |
| RCF | Relative centrifugal force |
| RNA | Ribonucleic acid |
| RNS | Reactive nitrogen species |
| ROS | Reactive oxygen species |
| SDBS | Sodium dodecyl benzene sulfonate |
| SDS | Sodium dodecyl sulfate |
| ssDNA | Single-stranded DNA |
| STA | Surface-tethered alginate |
| SWNT | Single walled carbon nanotubes |

| | |
|---|---|
| uPA | Urokinase plasminogen activator |
| UV | Ultraviolet |
| UV-Vis | Ultraviolet-visible |

TABLE OF CONTENTS

# LIST OF FIGURES

# LIST OF TABLES

# CHAPTER 1

## Introduction, Background, Objectives

### 1.1 Introduction

The term biosensor describes a wide variety of molecules and devices that are capable of converting biological cues and information into detectable signals for analytical purposes.[1] As such, biosensors are essential tools for researchers when attempting to expand current knowledge of biochemical pathways, fully detail core signaling cascades, and correlate deviations from homeostasis with disease states.[2] By increasing the characterization and knowledge of key biological processes, researchers will be able to develop tests for earlier disease detection and more targeted therapies and interventions. The term biosensor was first coined in 1977, referring to an enzymatic-based detection scheme.[3] Since then, the field has expanded to include sensors based on cells or tissues, immune system components, DNA, magnetic forces, thermal fluctuations, piezoelectric accumulation, and optical shifts.[1, 4-10] However, even with the expansion of detection schemes, useful biosensors all maintain a core set of functions: stability, high target specificity, biocompatibility, and limited nonspecific interaction.[11-16]

One of the more recently developed classes of biosensors is optical biosensors, which have seen an exponential rise in attention from researchers in the past two decades.[17] Optical biosensors are attractive due to their sensitivity, detection rate, non-invasive detection, and non-destructive employment.[18-20] One hindrance to this type of sensor is the penetration of light through biological media such as water, blood, cells,

and tissue, which has led researchers to focus attention on expanding optical biosensors into the infrared (IR) portion of the electromagnetic spectrum.[21-25] Tissue penetration depth increases directly with wavelength as visible light (380-700 nm) has an estimated maximum penetration depth of 100 um and near infrared (nIR) light (900-1700 nm) can penetrate 3 cm.[18, 21-23, 25-30] The massive increase in tissue penetration depth of near infrared light is due to the off resonance frequency of the light with water, leading to less interference through biological matter.[31] Most optical biosensors function in a similar manner, excitation light is used to change the sensor into an excited state, and subsequent relaxation releases the stored energy as a less energetic photon. To this end, the shift towards the red end of the spectrum not only allows for better emission signal penetration, but also shifts the required excitation lights away from the low-visible/UV region of the spectrum.[28, 32] This shift away from blue light can lengthen sensor lifetime by preventing photobleaching effects and alleviating phototoxicity concerns from UV light interacting with biological systems.[33-40]

One particularly interesting class of near-infrared optical biosensors is single walled carbon nanotubes (SWNT). SWNT have a unique electronic structure that makes them advantageous over other nIR fluorophores while maintaining all of the key characteristics of useful biosensors previously outlined. Unfortunately, applications towards clinical translation of these promising biosensors have been limited. **Key factors preventing translation are biocompatibility concerns due to a lack of fate determination, complex detection schemes that are incompatible with large animal models, and localization strategies that affect sensitivity.** Chapters 2-4 address each one of these concerns, providing insights into the underlying mechanisms of each factor

and possible avenues for circumvention. In order to better understand SWNT sensors and the key factors preventing clinical translation, the rest of Chapter 1 is focused on SWNT sensor development and function as well as background information on SWNT sensor platforms, biocompatibility concerns of SWNT in biological settings, and applications of SWNT sensors.

### 1.2 Single Walled Carbon Nanotubes

Pure carbon structures are vastly different depending on the electronic dimensionality of the structure. A two-dimensional sheet of carbon is referred to as graphene, while layers of graphene create a three-dimensional structure known as graphite. Conceptually, a single walled carbon nanotube is a rolled up sheet of graphene with a diameter of 0.5-2 nm.[41] SWNT are thought of as a one-dimensional carbon structure as dimensionality refers to the electronic structure, not necessarily the actual shape. The electrons in graphene are able to move in two-dimensions along the face of the pure carbon sheet, whereas in graphite the electrons are free to move into other layers of graphene, providing a third dimensionality. In SWNT the electrons are confined to movement along the axis of the nanotube, and it is this one-dimensional quantum confinement of the valence electrons that leads to the unique electronic and optical properties of SWNT.[41]

There are many varieties of carbon nanotubes (CNT), including multiwalled (MWNT) and single walled, and there are many different structures within each type. MWNT are frequently used for electronics and as structural components in composite

materials, the focus of this work is using SWNT and, unless otherwise stated, the rest of this work will be referring to SWNT not MWNT when discussing CNT.

The major differences between SWNT can be seen in the orientation of their $sp^2$-bonded hexagonal rings, with each nanotube variety denoted as a chirality having the nomenclature n,m. The n,m notation refers to the chiral indices of the carbon nanotubes and can be determined from the number of carbon atoms required to "roll-up" a sheet of graphene into the specific n,m chirality nanotube (figure 1-1).[42-45] The n,m orientation directly affects the SWNT properties as it is related to the diameter of the tube. SWNT can be metallic, semimetals, or semiconductors based on chirality.[42-44, 46] The SWNT used in this work were chiral and semiconducting.

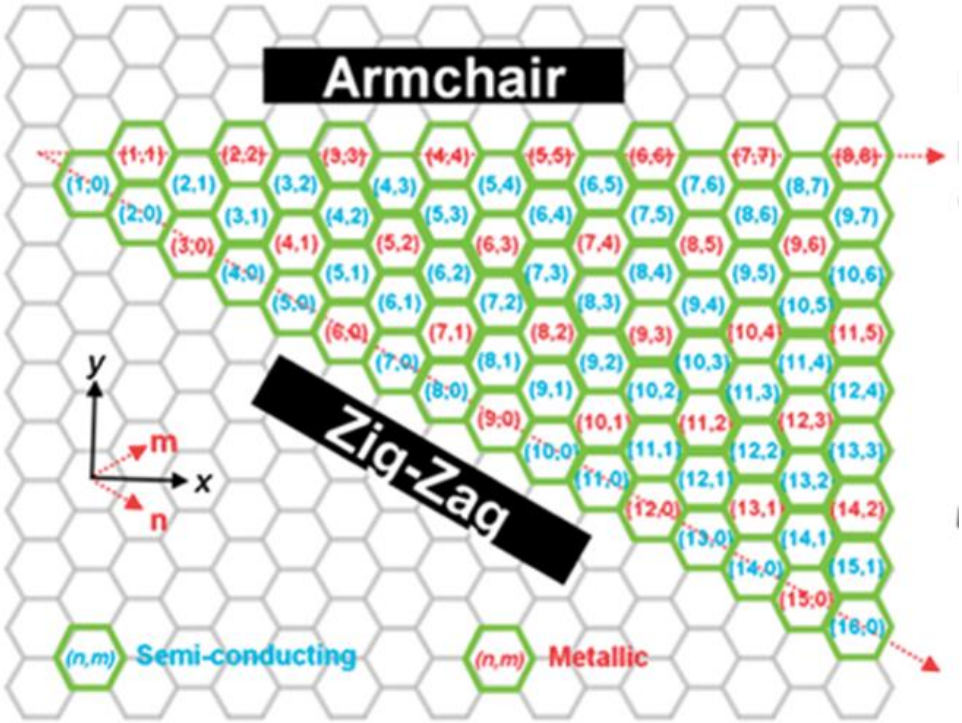


Figure 1-1: SWNT chirality. The n,m notation is used to describe the chirality of each individual carbon nanotube species and is determined from the number of carbon atoms in each direction along the

circumference. The chirality of SWNT is directly related to its diameter and therefore its electronic properties as electron confinement is inversely related to diameter. (Figure adapted from Hodge et al.[45] with permission from The Royal Society of Chemistry, Copyright © 2012).

### *1.2.1 Electronic Structure of SWNT*

Single walled carbon nanotubes owe their electronic structure and subsequent optical properties to the one-dimensional quantum confinement of their valence electrons. Graphite is a conductor meaning the valance band and conduction band overlap, but as the electrons become confined, as in the case of two-dimensional graphene or one-dimensional SWNT, a band gap develops between the valence and conduction bands creating a semiconductor.[47] The density of states for various dimensionalities of semiconductors is described in figure 1-2. In the case of one-dimensional objects like SWNT, the electrons are found in distinct energy levels or bands. In a semiconductor the conduction band is close enough in energy to the valance band that transition of an electron is still possible given an excitation energy, usually in the form of heat or light. When an electron moves to the conduction band it leaves behind a positively charged electron hole in the valance band.[48] Together, the electron and electron hole form a quasiparticle called an exciton.[48] It is this electronic structure and formation of excitons that lead to the useful optical properties of SWNT, as radiative exciton recombination leads to photon emission in the nIR portion of the electromagnetic spectrum. The band gap for semiconducting SWNT is around 1 eV, which requires excitation to occur in the upper visible range (500-780 nm) and results in enough energy

being released during radiative exciton recombination to produce a photon in the nIR range (900-1700 nm).[24, 47, 49-53] The advantages of the nIR emission have been discussed, but the Stoke-shift between excitation and emission wavelengths for SWNT is also an advantage as the wide shift leads to decreased autofluorescence. [24, 44, 50, 54, 55]

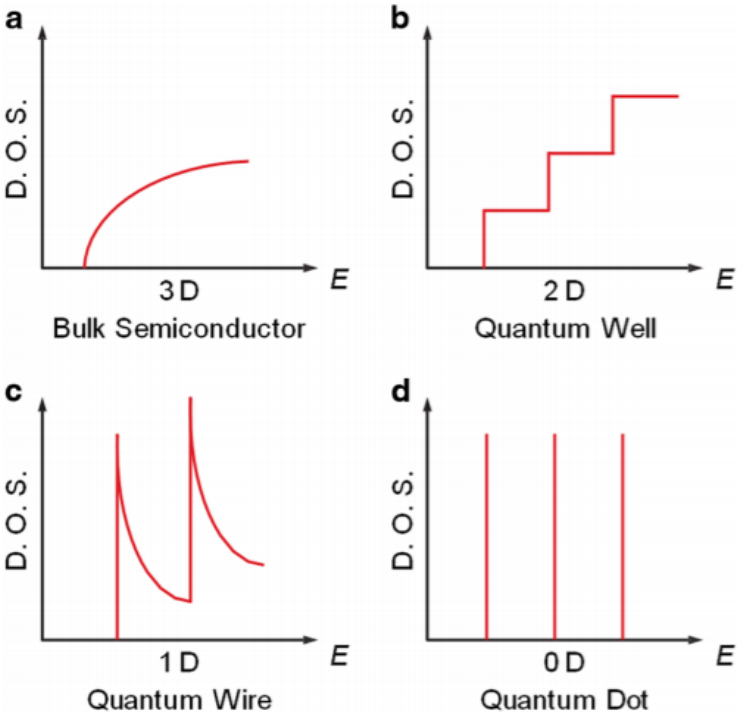


Figure 1-2 Density of states for semiconductors by dimensionality. The density of states plot is the result of solving the electron wavefunction for an infinite potential well for a unit volume. As the electrons become confined from 3D (a) to less dimensions, the equation begins to form specific energy levels. This discretization of the electrons location results in distinct levels for 2D (b) sharp peaks for 1D (c) and discrete points for 0D (d). SWNT are considered one dimensional due to the confinement of the electrons along the tube's axis. (Figure from Zhang et al. [56] open access article from Springer Nature, Copyright © 2017).

### *1.2.2 SWNT Sensor Development*

SWNT was first characterized in Japan by Sumio Iijima in 1991, however the band gap fluorescence was not reported until O'Connell et al.'s 2002 paper.[41, 49] Suspension of SWNT with sodium dodecyl sulfate (SDS) and poly(vinylpyrrolidone) (PVP) resulted in micelle formation around the carbon nanotubes. Subsequent characterization of the suspended SWNT led to the discovery that individually dispersed nanotubes experience one-dimensional quantum confinement and result in the band gap fluorescence that created the field of SWNT as optical biosensors.

Today, SWNT sensors are still created by noncovalent suspension of individually dispersed nanotubes, as covalent modification disrupts the one-dimensional quantum confinement of the electrons.[57] However, further steps have been taken to create SWNT sensors that are responsive to specific cues or analytes. Sensor creation is accomplished by both limiting the interactions of the nanotube with its environment, steric hindrance, and by redox selectivity.[58] Steric hinderance is accomplished by noncovalently wrapping the nanotube with a polymer or surfactant that act as a physical barrier between the nanotube and molecules in the surrounding medium [58]. In the case of the nitric oxide (NO) sensing SWNT, which is the sensor used in this work, single-stranded DNA is used to create a barrier that still allows the NO molecule to interact with the nanotube while blocking many other biologically relevant molecules. Selectivity of the small molecules that can still interact with the nanotube is accomplished by redox sensitivity, which is a process in which free radicals of a certain valance energy can modulate the SWNT electronic structure.[58] As previously stated, the fluorescence from

SWNT is produced from radiative exciton recombination, however; in the presence of NO the fluorescence is quenched.[58-61] The observed quenching is due to the lowest unoccupied molecular orbit (LUMO) of NO having and energy level that falls in the band gap of the SWNT just below the conduction band. Under normal circumstances the LUMO is the conduction band, resulting in fluorescence from radiative exciton recombination as previously stated. In the case of SWNT with NO, the LUMO is now the unpaired free radical orbital of the reactive nitrogen species, in this way the NO absorbs the electron that would have moved to the conduction band. Since the NO energy band lies within the band gap there is less energy involved in the transition and an exciton is not formed resulting in an overall loss of radiative exciton recombination and a quenching of the fluorescence (figure 1-3).

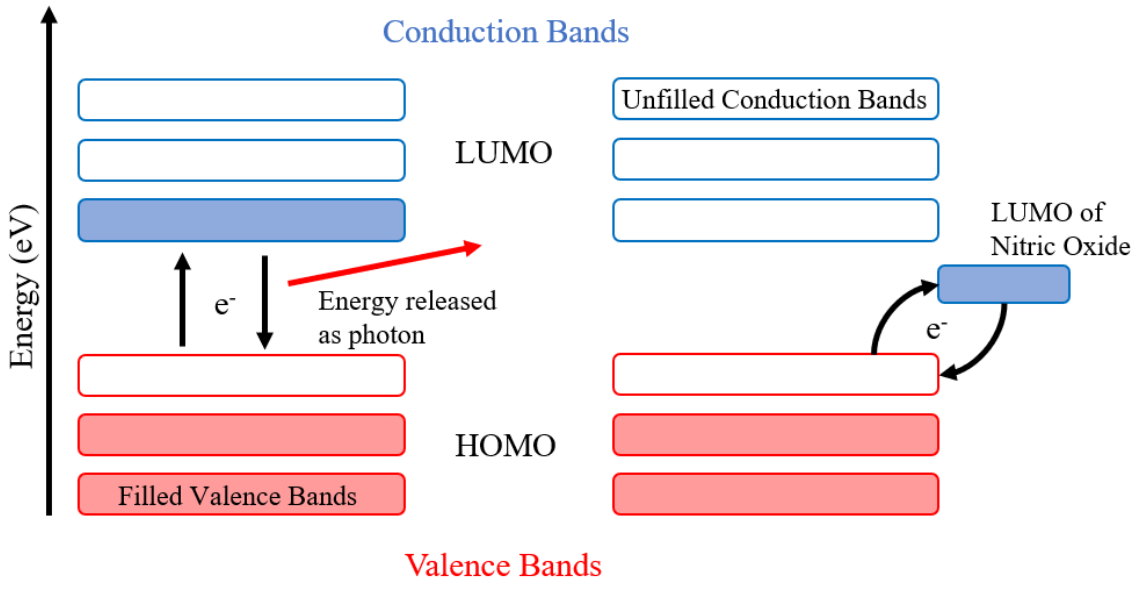


Figure 1-3: NO sensing SWNT. Electrons under normal conditions in the presence of excitation light will move from the valance band (HOMO-Highest occupied molecular orbital) of SWNT to the conduction band (LUMO). Subsequent radiative exciton recombination results in emission in the nIR. When nitric

oxide is introduced, the excited electron still moves to the LUMO, however; in this case the LUMO is now the unoccupied orbital on the NO rather than the conduction band of the SWNT. Since the LUMO of the NO is closer to the SWNT in energy, an exciton is not formed and there is no radiative exciton recombination i.e., a quenching of the fluorescence occurs.

After creation of SWNT sensors is accomplished by noncovalent functionalization by an amphiphilic polymer wrapping, the fluorescence response to the target analyte is investigated. The SWNT fluorescence is either red- or blue-shifted (the energy of the excitons is changed) or the signal is attenuated or amplified (redox reactions lead to more or less exciton formation).[62]

Recently, novel detection schemes have emerged including solvatochromic shifts based on the surrounding media, large molecule detection via p-doping/n-doping, and aptamer-anchor designs with a polymer anchor and binding domain for analyte detection.

Solvatochromic shifting is a phenomenon where the solvent that a substance is dissolved in can shift the spectrum of that substance. Harvey et al. used this property in conjunction with SWNT to detect alkylating agents via controlled solvatochromic shifts in SWNT fluorescence.[63] The alkylating agents, commonly used chemotherapy drugs, would covalently interact with the DNA wrapping on the SWNT, causing a conformational change that exposed the nanotube to the environment. The group found that the medium that was employed could control the observed shift in fluorescence once the nanotube had been exposed by the alkylating agent. It was discovered that the intensity and wavelength shifts could be manipulated by the solvent. Solvatochromism offers and avenue to tailor SWNT sensor response, allowing for optimal signal detection.

Large molecule detection via SWNT sensors has remained more difficult and previous attempts at glucose detection relied on large wrapping domains that were irreversibly altered by glucose interaction, limiting application. In response, a novel glucose sensor was developed using a scheme of enzymatic pocket doping with glucose oxidase wrapped around SWNT.[64] Incorporation of the enzyme created oxygenated p-doped sites on the nanotube, decreasing fluorescence intensity. Upon addition of glucose the glucose oxidase underwent oxidation resulting in n-doping of the SWNT and observed increases in fluorescence.

Finally, an aptamer-anchor approach has been developed where a polymer "anchor" is covalently linked to an aptamer binding domain. The polymer works to wrap and disperse the SWNT while also anchoring the aptamer binding domain to the nanotube. When the target analyte is introduced the aptamer will bind the analyte, causing a conformational change in the wrapping that impacts the SWNT dielectric environment and results in an emission change. One such sensor was developed for the detection of insulin using a single-stranded DNA (ssDNA) anchor and an insulin binding aptamer.[65]

Many novel detection schemes are being developed every year that rely on target analyte interaction with either the SWNT dielectric environment directly, or conformational changes of the SWNT dielectric environment through the wrapping. Simple modification of the wrappings or binding domains of these schemes result in sensors for various analytes and the SWNT sensor library is rapidly expanding (table 1-1). The library now includes SWNT sensors for neurotransmitters, small reactive molecules, proteins, key signaling molecules, viruses, and genetic material.

Table 1-1. SWNT sensor library.

| Analyte Targeted | Functionalization | Reference |
|---|---|---|
| **Ag+ and cysteine** | FAM labeled 5'-CTC TCT CTC TCT CTC TCT CTC-FAM-3' | [66] |
| **Arsenite** | $(GT)_5$ | [67] |
| **Avidin** | Dye ligand conjugates doped SDS micelles | [68] |
| **Catecholamines (DA and NE)** | $(GT)_6$ | [69] |
| **CD20 cell surface receptor** | PEG-Rituxan | [70] |
| **$Co^{2+}$ $Ca^{2+}$ $Mg^{2+}$** | $d(GT)_{15}$ | [71] |
| **DNA hybridization** | 5'-TAG CTA TGG AAT TCC TCG TAG GCA-3' | [72] |
| **Dopamine** | $(GA)_{15}$ | [73] |
| **Doxorubicin** | $(GT)_{15}$ | [74] |
| **Estradiol** | RITC-PEG-RITC | [75] |
| **Glucose** | B-D-glucose | [76] |
| **Glutathione-S-transferase** | $(TAT)_6$-GSH | [77] |
| **HER2/neu** | PEG- Herceptin | [70] |
| **$Hg^{2+}$** | $d(GT)_{15}$ | [71] |
| **HIV RNA** | $(GT)_{15}$-$(T)_{15}$ | [78] |
| **HIV1 integrase protein** | $(AT)_{11}$-HIV-1 aptamer complex | [79] |
| **human IgG, mouse IgM, rat IgG2a, and human IgD** | Chitosan/immunoglobulin-binding protein complex | [80] |
| **Hydrogen Peroxide** | $d(GT)_{15}$ | [17] |
| **Hydrogen Peroxide** | Collagen | [81, 82] |
| **Insulin** | PEGylated lipid heteropolymer | [83] |
| **L- Thyroxine** | Fmoc-Phe-PPEG8 | [75] |
| **LDL Cholesterol** | 5'-CTTC3TTC-3' | [84] |
| **Lectin protein WGA** | (Nce-Npe)-PC36 | [85] |
| **Lipids** | $(GT)_6$ | [86] |
| **miRNA Hybridization** | $(GT)_{15}$-miRX | [87] |
| **Microalbuminuria** | Carboxy-PCD | [88] |
| **Nitric Oxide** | $d(AT)_{15}$ | [58] |
| **Nitric Oxide** | DAP-DEX | [59] |
| **Progesterone** | Acrylated cortisol | [89] |
| **RAP-1 Protein** | $(AT)_{11}$-RAP1 aptamer complex | [79] |
| **Riboflavin** | $(AC)_{15}$ | [90] |
| **Riboflavin** | BA-PhO-Dex | [75] |
| **SARS-CoV-2 spike protein** | $(GT)_6$-ACE2 | [91] |
| **Serotonin** | $C_6$-N18-$C_6$ | [92] |
| **Single nucleotide polymorphisms** | 5'–TAGCTATGGAATTCCTCGTAGGCA – 3' | [93] |
| **Troponin T** | Chitosan/anti-troponin antibody complex | [94] |
| **Tyrosinase activity** | $PEG_{12}$–$GT_{15}$–amine | [95] |
| **Vardenafil** | Poly(methacrylic acid-costyrene) | [96] |

## 1.3 SWNT Sensor Applications

SWNT sensors are being applied for *in vitro*, *ex vivo*, and *in vivo* detection of key biological analytes. This section will explore some of the more recent publications in each of these areas.

### *1.3.1 In vitro*

Cellular research has led to important discoveries that apply on a system wide scale, whether it be a tissue or whole organism. As such, there is a need for extracellular and intracellular sensors, and recent research with SWNT sensors has aimed to address this need.

Using SWNT-based sensors, researchers were able to show dopamine excretion from neuroprogenitor cells and actually map the dopamine in real time.[73] A SWNT sensor, based on ssDNA wrapping, that is capable of dopamine detection was immobilized and neuroprogenitor were seeded on top of the sensing platform. After stimulating the cells to excrete dopamine, hyperspectral imaging allowed for real-time mapping of the analyte. Another study investigated serotonin release from cells by employing an anchor-aptamer-type SWNT sensor in a similar manner, with the cells being directly seeded on a SWNT sensing platform.[97] High spatial and temporal monitoring of serotonin was accomplished, and offered insight into cell to cell signaling, an often difficult task to accomplish due to signaling molecule size and half-life.

Intracellular detection is difficult due to the complexities with localizing sensors to specific proteins or organelles and the dynamics of the cell lifecycle. One group made

a major stride towards enhanced intracellular sensing by complexing SWNT with guanidinium-functionalized helical polycarbodiimide, which allowed for transport of the SWNT into the cell nuclei.[98] The SWNT complexes entered the nuclei of HeLa cells via importin β-mediated transport, and upon entry into the nuclei the SWNT underwent a distinct red-shift, creating a sensor for a specific mediated pathway to the nucleus of a cell.

### *1.3.2 Ex vivo*

The most common use of *ex vivo* SWNT sensors is to achieve high throughput screening of biological media for key analytes and biomarkers. An anchor-aptamer type SWNT complex sensitive to insulin was developed using $C_{16}$-PEG-ceramide polymer.[83] The researchers discovered the PEG-ceramide only displayed affinity for the insulin when wrapped around the SWNT indicating a "molecular recognition" by the SWNT rather than a nonspecific interaction. A strong fluorescence quenching of the SWNT signal was observed in both an aqueous solution and serum when insulin was added. Another anchor-aptamer-type SWNT sensor was developed for the RAP1 protein, displaying the versatility of this detection scheme.[79] The RAP1 aptamer was bound to the SWNT by a ssDNA anchor and displayed a dose dependent increase of SWNT fluorescence intensity when RAP1 was added to the system. The fluorescence modulation was sensitive enough to allow single molecule detection of RAP1 in serum.

A carboxy-polycarbodiimide (PCD) wrapped SWNT was developed for the detection of microalbuminuria in urine.[88] This analyte is a marker for a number of

cardiovascular disease states, such as hypertension and atherosclerosis, and other diseases such as diabetes and cancer. The PCD-SWNT sensor was incorporated into a nanosensor paint to create a cheap and portable nanosensor array for screening urine outside the laboratory.

A sensor for a biological marker of metastatic prostate cancer, urokinase plasminogen activator (uPA), was developed using and antibody incorporated wrapping.[99] A dose dependent red-shift of SWNT fluorescence was observed in response to the biomarker in bovine serum, human serum, and human plasma.

Finally, a sensor for HIV was developed using ssDNA wrapping on SWNT that was amplified by denatured proteins.[78] The sensor was specific to the virus RNA, with the addition of denatured proteins in serum amplifying the observed blue-shift of the SWNT in response to the virus RNA. The amplification was attributed to the interaction of the denatured proteins with exposed hydrophobic sections of the nanotube following detection of the RNA.

### *1.3.3 In vivo*

*In vivo* applications of SWNT sensors are an exciting area of research as the field tries to move towards clinical applications and long-term sensing of key biological analytes and markers.

Rodent models have seen extensive study with SWNT sensors, and a sensor for lipid accumulation in the endolysosomal lumen of mice was developed using a ssDNA wrapped SWNT.[84] SWNT sensitive to various lipid species, including cholesterol,

sphingomyelin, and oxidized LDL, showed *in vivo* detection and biocompatibility. Another study showed successful *in vivo* detection of human epididymis protein 4 (HE4), an ovarian cancer biomarker.[100] The sensor complex consisted of SWNT wrapped with a ssDNA anchor and anti-HE4 IgG antibody that demonstrated a dose dependent blue-shift in response to HE4 injections into a live mice. Finally, doxorubicin was detected in mice with ssDNA wrapped SWNT in both subcutaneous and intraperitoneal sensing platforms.[74] In both case a dose dependent red-shift of the SWNT signal was observed in response to doxorubicin, marking the first ever successful nondestructive detection of the analyte *in vivo*.

Tissue penetration has remained an obstacle for optical probes over the years, the Weisman group overcame this obstacle by developing a new detection setup using multiple detectors, called spectral triangulation. In this study, researchers loaded SWNT into Matrigel and implanted the SWNT-gels into mice ovaries.[101] The live mice were then placed on an LED platform for excitation and a nIR detector array was used to collect emission from the SWNT through the mouse body. Using this setup, researchers were able to obtain imaging depths of 1 cm using a relatively small volume of sensor. Another group chose to address tissue penetration by focusing on the excitation light. Two-photon excitation was used to excite HiPco SWNT wrapped with ssDNA by loading SWNT sensors that was placed in capillary tubes and implanted in phantom brain tissue.[102] The two-photon 1560 nm excitation source resulted in only a 4% scattering of the sensor emission through the mimic, with similar results *in vivo*.

## 1.4 Biocompatibility

The biocompatibility of CNTs has been a widely debated issue in the scientific community for two decades. As of the writing of this work, there have been over 350 published works concerning CNTs and toxicity/biocompatibility. This section will explore the conflicting reports and offer insight into the negative stigma surrounding SWNT and biocompatibility.

### *1.4.1 Toxicity*

There is consensus among many scientists that CNTs are generally toxic, as many reports have come out over the past two decades supporting this notion.[103-105] However, during the same time period many reports concerning the biocompatibility of SWNT have also been published.[106-108] Both arguments are correct, as reports have shown nanotubes to lead to negative, neutral, or even positive effects when used with cells, tissues, or organisms. The toxicity or biocompatibility of CNTs is dependent on a variety of factors including the type, size, and structure of nanotube used, as well as preparation techniques and avenue of administration.[109-111] For example, MWNT tend to aggregate in the lungs and have been shown to cause asbestos-like effects in mammals, while functionalized SWNT have been used as sensors in a variety of live animal and cell studies with no adverse effects and have even been implanted into mice for 400 days without causing an inflammatory reaction.[105, 112] It is this miscommunication of situational toxicity and biocompatibility that leads to the negative stigma surrounding the umbrella term of carbon nanotubes.

Recently, carbon nanotubes were added to the SIN (substitute it now) list by the advocacy group ChemSec as a nanomaterial of very high concern.[103] The entirety of carbon nanotubes as a material class were recommended by ChemSec to be restricted or banned in the European Union. The blanket addition of all carbon nanotubes to the SIN list was based on a narrow subset of CNTs with a focus on MWNTs and early toxicology reports.[104, 105] The early toxicology reports were based on a bolus injection of long, insoluble nanotube aggregates that led to lung toxicity in mice. Unfortunately, these early toxicology reports received much traction and created an early stigmatized view of carbon nanotubes, and it is with this lens that ChemSec made their decision to add carbon nanotubes to the SIN list as a nanomaterial of very high concern.

### *1.4.2 Response*

The nanotechnology community, especially SWNT researchers, responded to the addition of carbon nanotubes to the SIN list by citing the many reports concerning the biocompatibility of functionalized, short, and soluble carbon nanotubes that have been applied to a growing number of biological systems.[113] In fact, following the original toxicology reports of CNTs there were reports demonstrating the biocompatibility of short soluble SWNT in primates; however, the reports concerning the biocompatibility of SWNT did not receive the same attention as the reports on toxic effects.[114]

The articles outlined in section 1.3 provide evidence towards the biocompatibility of SWNT sensors and add to the growing list of successful applications in cells and tissues with little or no adverse effects. Recently, a study was performed concerning the

biocompatibility and fate of SWNT wrapped with ssDNA in a mouse model.[115] Researchers injected the mice with ssDNA wrapped SWNT and monitored organs of interest such as the liver, kidney, spleen, lung, and heart. They were able to conclude short and long-term biocompatibility based on histology, animal weight, complete blood count, and biomarkers of organ function. Predictably, the study found an accumulation of SWNT sensors in the liver with eventual clearance of ~90% of the nanotubes.

Due to the conflicting reports concerning the toxicity and biocompatibility of SWNT, coupled with the negative stigma perpetuated by the addition of carbon nanotubes to the SIN list, at the moment, the safest route of sensor translation is through biocompatibility studies for each type of SWNT and each delivery method. Chapter 2 will focus on the biocompatibility of 6,5 chirality carbon nanotubes wrapped in $(AT)_{15}$ ssDNA applied via hydrogel to a sheep model.

### 1.5 Large Animal Models

An immense amount of research has been performed with SWNT sensors in mice models since 2013, the date of the first localization of SWNT sensors in a mammal, and has led to the development of detection schemes and the growth of the sensor library.[112] However, translation of SWNT sensors to the clinical setting will require models in large animals.

### *1.5.1 Advantages over Rodent Models*

Mouse and rat models offer researchers a convenient and effective method for developing and testing key concepts and interventions with the potential to translate results to humans. Rodents have long been a popular model for biomedical research due to their fast and easy breeding allowing for selection and generation of specific condition models rapidly.[116] However, rodent models do not represent the anatomy, physiology and immunology of humans very well.[117] Additionally, the size differences of these models when compared to humans makes significant changes to administration of components and interventions in biomedical research, confounding the results.[116] Sheep models have been more successful at mimicking human conditions as the animals are closer genetically and in size to humans. These qualities make the treatments and interventions more representative of what they would be in a clinical setting, providing more valuable data for translational research.

### *1.5.2 Difficulties*

While sheep tend to be better models for humans in biomedical applications, their applications are few and far between. The relative cost of a large animal study is much higher due to the longer lifespans and increased size of the test subjects.[116] The animals must be housed and fed for the duration of the study which requires significant dedicated space and large amounts of food.[116] Additionally, commonly used techniques to restrain rodents, like “scruffing”, are not applicable to larger animals. Large

animals frequently require multiple individuals to handle the animals and a restraint system for acquiring measurements. Finally, nanotechnology systems are typically complex and immobile, making field measurements on large animals impossible.

Chapter 3 of this work focuses on the development and characterization of a relatively simple and portable setup for the detection of SWNT sensors in the field. Furthermore, access to a top tier animal housing facility in the University of Nebraska-Lincoln's Animal Science Complex allowed for the first signal detection of SWNT sensors in a large animal.

### 1.6 SWNT Sensor Localization

Localization of biosensors *in vivo* has been a goal for researchers for decades, since long-term *in vivo* biosensing would give medical providers real-time data on patient health and lead to improved personalized care.[118] The long-term monitoring would provide information on basal levels of various factors for a specific patient and any then more accurately detect deviations that are consistent with impending disease. *In vivo* biosensing would also provide valuable information about efficacy of treatment, allowing providers to optimize dosing to avoid potentially damaging side effects or ineffective interventions due to high or low dosing. SWNT sensors are a potentially optimal platform for long-term sensing due to the characteristics outlined above, specifically, stable nIR fluorescence, adaptability to various detection schemes, and interchangeable functionalization for rapid analyte-sensor pairing. However, SWNT sensors must be localized via some platform as a bolus injection of suspended SWNT sensors results in accumulation in filtering tissues, such as the liver and kidney, or sensor clearance.

### *1.6.1 Platforms*

The first *in vivo* experiment utilizing SWNT was in 2007 when researchers fed drosophila larva a diet consisting of functionalized SWNT.[119] Monitoring of fly health and fluorescence through the life cycle resulted in continuous SWNT fluorescence in the digestive tract with no adverse effects on organism health. It was not until 2013 that SWNT-based sensors were first applied to a mouse model when researchers used both bolus injections and hydrogel platforms to deliver the nanotubes.[112] The injected SWNT predictably accumulated in the liver of the mice, and the hydrogel platforms were successful at localizing SWNT sensors for 300 days. The responsiveness of the sensors to the target analyte, NO, was also assayed using a liver inflammation model, demonstrating that the injected sensors remained responsive to NO.

Since these original works made the leap into living organisms, much research has been done using SWNT as *in vivo* biosensors. The vast majority of *in vivo* applications of SWNT use hydrogel-based platforms in mice models.[89, 90, 118, 120] Hydrogels are the platform of choice due to their mechanical properties, which closely mimic native tissue, as well as their optical transparency, tunability, biocompatibility, and ease of incorporation of SWNT sensors. Additionally, researchers have explored other options to localize the sensors *in vivo* such as dialysis membranes and firmer synthetic implants based on silicon.[100, 121] However, concerns regarding longevity and irritation arise when using these types of platforms.

### *1.6.2 Sensitivity Concerns*

Although SWNT-hydrogel constructs have shown promise as a localizable nIR biosensing device, SWNT sensitivity is greatly impacted by the hydrogel matrix. A dramatic response-time delay was observed for sensors incorporated into the matrix of alginate hydrogels, which increased the time for the sensors to reach maximum response nearly tenfold (figure 1-4).[112] The sensors also took approximately 40 hours to recover their initial fluorescence as compared to less than 30 minutes for sensors in solution. The observed delayed response was hypothesized to be due to the interaction of the SWNT with the hydrogel. The observed delay not only impacts the temporal resolution of the sensors, but it also affects the spatial and spectral resolution, because the diffusion of the analyte is altered creating a local concentration gradient that is not reflective of the surrounding environment. Chapter 4 focuses on this effect and possible avenues of circumvention.

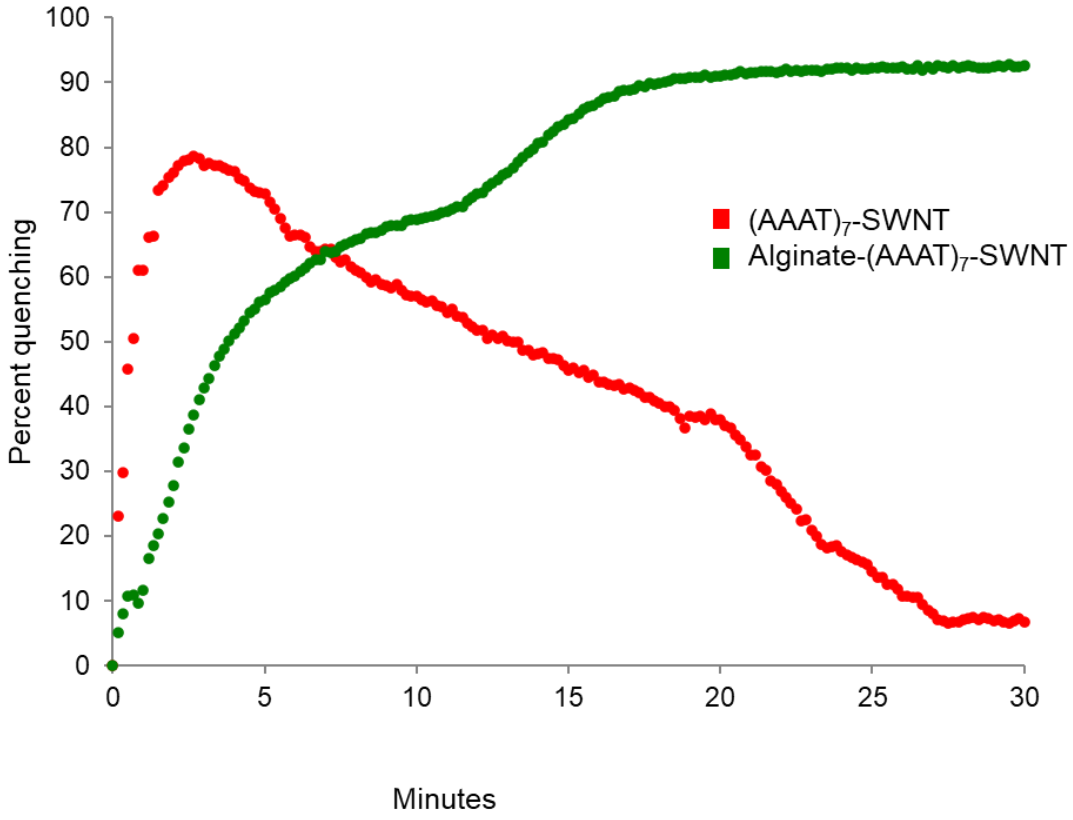


Figure 1-4. Delayed sensor response. Incorporation of SWNT sensors into the matrix of alginate hydrogels (green) results in a delayed response to the target analyte, nitric oxide, as compared to sensors in solution (red). The fluorescence quenching is delayed to twenty minutes and the recovery of the signal is delayed to over 40 hours. (Figure from Iverson et al. [112], with permission from Springer Nature, Copyright © 2013)

## 1.7 Dissertation Objectives

The research reported in this dissertation aims to move SWNT-based biosensors towards clinical application. Biocompatibility of SWNT-based sensors is a concern due to early toxicology reports and the possibility of noncovalent functionalization of sensors leading to removal of the SWNT wrapping, resulting in aggregation in filtering tissues. Chapter 2 of this work focuses on developing techniques to account for SWNT sensors implanted *in vivo* by extracting and quantifying nanotubes from hydrogels and tissues. Chapter 3

describes a relatively inexpensive and portable setup that demonstrated signal detection of SWNT sensors in a large animal model for the first time. Finally, chapter 4 focuses on the interaction between the target analyte, sensor, and hydrogel platform in order to create a real time implantable sensor for long-term localized biosensing.

# CHAPTER 2

## Novel Methods to Extract and Quantify Sensors based on Single Wall Carbon Nanotube Fluorescence from Animal Tissue and Hydrogel-Based Platforms

### 2.1 Abstract

Sensors that can quickly and accurately diagnose and monitor human health are currently at the forefront of medical research. Single walled carbon nanotube (SWNT) based optical biosensors are a growing area of research due to the high spatiotemporal resolution of their near infrared fluorescence leading to high tissue transparency and unparalleled sensitivity to analytes of interest. Unfortunately, due to the functionalization requirements of SWNT-based sensors, there are concerns surrounding accumulation and persistence when applied *in vivo*. In this study, we developed protocols to extract and quantify SWNT from complex solutions and show an 89% sensor retention by hydrogel platforms when implanted *in vivo*. Animal tissues of interest were also extracted and probed for SWNT content showing no accumulation (0.03 mg $L^{-1}$ SWNT detection limit). The methods developed in this paper demonstrated one avenue for applying SWNT sensors *in vivo* without concern for accumulation.

### 2.2 Introduction

The need for fast and accurate sensors that can detect and monitor human health has become even more apparent in the recent months, but if a sensor is not biocompatible, it cannot be used in humans. Without performing long-term animal studies that investigate the impact of new sensors over multiple decades, it is possible that injected or implanted

sensors will result in negative long-term side effects. One way to avoid this issue is to deliver sensors in a biocompatible platform that will allow for interaction between blood and the sensors, but not allow the sensors to be released into the blood stream or surrounding tissue. Many types of hydrogels are known to be biocompatible and serve as excellent platforms for sensor delivery; however, in the case of nanosensors, precise measurements of sensor concentration pre-implantation and post-excision must be performed to ensure retention. In this paper we will explain two new methods for analysis of nanoparticle retention by hydrogels after *in vivo* implantation.

The nanoparticles used in this study are single walled carbon nanotubes (SWNT), but other nanoparticles could also be analyzed with these methods. Many nanoparticles and nanomaterials are based on silicon and carbon, which largely form hydrophobic complexes. The methods developed in this work rely on the hydrophobic nature of the nanoparticles to isolate them from complex aqueous solutions for future quantification, therefore the isolation of non-SWNT nanoparticles could be accomplished with similar methods.

SWNT are pure carbon structures of ~1 nm in diameter with lengths varying from ~100 nm to multiple cm depending on the fabrication and functionalization processes[122-125]. There are three distinct structures of SWNT, known as armchair, zigzag and chiral nanotubes, but in this paper, we will be using chiral SWNT due to their fluorescence properties. When chiral SWNT are excited by visible (~400-700 nm) light they emit fluorescence in the near infrared (nIR) (900-1200 nm) range[24, 44, 51, 126-128]. The nIR fluorescence emitted by the SWNT falls within the tissue transparency window, wavelengths at which neither blood nor water have a high light absorbency,

making SWNT ideal particles for *in vivo* applications[24, 52]. SWNT are hydrophobic due to the aromatic carbon structure, which is not optimal for biological settings, and requires functionalization with polar moieties if they are to be used in an aqueous environment [17, 53, 129]. Typically, a hydrophobic particle can be conjugated with hydrophilic components to allow for dispersion in a polar solution and increased biocompatibility, but covalent bonds onto the SWNT surface impede fluorescence[57, 127]. Therefore, functionalization of SWNT must be accomplished via noncovalent means in order to preserve nanotube fluorescence while allowing for suspension within biological media[130]. This noncovalent dispersion can be accomplished by amphiphilic molecules such as surfactants, polymers, and DNA oligos[58, 73, 79, 81, 131-134].

Functionalization of SWNT by amphiphilic molecules not only allows for dispersion into biological media, but it also imparts selectivity by sterically hindering interaction between biological molecules and the nanotubes. SWNT sensors for various biological components, including insulin, glucose, nitric oxide, dopamine, and specific RNA and DNA segments have been developed[58, 59, 61, 65, 69, 71-73, 78, 83, 87, 100, 102, 131, 135, 136]. Carbon nanotube-based fluorescence sensors are advantageous due to the high spatiotemporal resolution they can provide and their ability to monitor analytes over long time periods (multiple months)[68, 112, 137]. The sensors rapidly respond to their target analyte with some predictable fluorescence modulation, including attenuation or amplification of the intensity or a red or blue shift of the peak wavelength[74, 99]. Following the removal of the target analyte, the SWNT sensor's signal returns to the initial intensity or wavelength, making SWNT a rapid and reversible sensing platform[64, 68]. Recent advancements in SWNT sensors for *in vivo*

applications, include the detection of lipid accumulation in the endolysosomal lumen of mice, the detection of the ovarian cancer biomarker human epididymis protein 4 in mice, the detection of nitric oxide in inflamed mouse livers, and the targeted delivery and adherence of dopamine sensing SWNT to the motor protein kinesin-5 in developing drosophila embryos[100, 112, 136, 138]. Unfortunately, without long-term monitoring of subjects following these experiments, it is unknown if and where SWNT will accumulated in the body or how potential SWNT accumulation could impact cells and tissues if dissociated from the amphiphilic wrappings. SWNT sensors localized to a platform that is removable and retrievable would avoid long-term exposure and accumulation concerns.

Sensors for nitric oxide (NO), specifically SWNT wrapped with $(AT)_{15}$ single-stranded DNA (ssDNA), were used to demonstrate the feasibility of novel methods for SWNT extraction and quantification from hydrogels. NO is a biologically active molecule known for its role in the cardiovascular system, specifically vasodilation, but it is also a key component of the gastrointestinal tract, nervous system, and immune system[139-142]. NO is involved in many processes, but it is not fully understood because sensing is difficult due to the high reactivity (short half-life) and small size of the molecule[143, 144]. With the spatiotemporal resolution of SWNT *in vitro* and *in vivo* the roles of NO can be studied and better understood.

In this study, SWNT sensors were incorporated into alginate hydrogels, assayed for concentration, and subcutaneously implanted into the ears of sheep. Following three weeks *in vivo*, sensors were excised, and novel extraction and quantification methods

were employed to determine SWNT retention by the hydrogels and SWNT accumulation within the animal.

## 2.3 Animal Use

All animal protocols and handling were approved by the Institutional Animal Care and Use Committee at the University of Nebraska-Lincoln [Protocol No. 1751].

## 2.4 Methods

### *2.4.1 SWNT sensor fabrication*

Single wall carbon nanotubes were purchased from Sigma Aldrich ((6,5) chirality, 0.7-0.9 tube diameter, carbon <95%, >93% carbon as SWNT) and ssDNA ($d(AT)_{15}$ oligo) was purchased from Integrated DNA Technologies (IDT). SWNT sensors were prepared according to previous experiments[58, 112, 145]. In brief, SWNT was suspended in 1:2 mass ratio with ssDNA in normal saline. Resulting suspension was bath sonicated (Bransonic, M2800H) for 10 minutes to separate SWNT bundles followed by ultra-sonication with a 3 mm probe tip sonicator (QSonica Q125 Sonicator) for 40 min to disperse individual nanotubes. The solution was then centrifuged (Beckman Coulter Microfuge 16) for 180 min at 16100 RCF and to remove any unwrapped SWNT and the supernatant was collected. The resulting nanotube sensor suspension was then diluted 10fold and UV/vis spectrometry (Beckman Coulter DU730) was used to determine concentration as described previously[58].

*2.4.2 SWNT-Alginate Hydrogel*

Alginate (Protanal RF 6650) was dissolved at 3% w/v in normal saline and SWNT sensor suspension was diluted to 30 mg $L^{-1}$. The two solutions were mixed to create a final 2% alginate solution with 10 mg $L^{-1}$ SWNT sensors. The resulting alginate-SWNT precursor solution was filled into a 10 mm diameter dialysis membrane (Fisherbrand, MWCO 3,500 d) to form a 10 cm long tube. The tube was then placed into a beaker containing 0.1 M $CaCl_2$ for crosslinking. The precursor solution was allowed to crosslink for 24 hours in the calcium chloride solution. The tube hydrogel was removed from the dialysis membrane and cut into 3 mm thick discs. The hydrogels were stored in normal saline at room temperature prior to implantation.

*2.4.3 Hydrogel Imaging.*

SWNT-hydrogels were photographed, and fluorescence intensity was recorded using a custom built nIR hyperspectral microscope (Photon Etc.). The custom-built microscope excites the sample using a 2 W laser (561 nm) and records emission signal using a volume Bragg grating to specify wavelength and an InGaAs camera to record the signal. An in house developed script using PhySpec (microscope software) was used to scan across the gel surface and record the intensity values for each pixel at 990 nm. The resulting 990 nm images were stitched together in MATLAB to form an overall fluorescence image for the gel.

*2.4.5 Implantation in sheep ears*

9 wether (<1 year old, castrated male) sheep were selected to receive implants. Hydrogels were placed subcutaneously in sheep ears by or under the supervision of a trained veterinarian and closed with suture. Each sheep was given 2 hydrogels, one gel containing the SWNT sensors, and one gel containing only alginate. Prior to surgery animals were treated with sheers and commercial hair remover to remove excess hair/wool from the implantation sites. Two pockets were created, one on each ear. The gels were placed into the pockets and the incisions were closed.

*2.4.6 Hydrogel recovery and tissue extraction.*

Following a three-week period, the animals were sacrificed, and tissue was collected in accordance with IACUC guidelines. Briefly, animals were stunned using a pneumatic device and sacrificed by exsanguination. The ears were removed, and hydrogels were extracted from the implantation sites. Finally, the organs were removed from the animal and the organs of interest were collected (lungs, spleen, heart, liver, and kidneys).

*2.4.7 Degradation of hydrogels.*

Hydrogel implants were degraded to perform later experiments. Alginate hydrogels were mixed into and incubated with alginate lyase (Sigma Aldrich, 25 U) at 37 C for 24 hours to breakdown the gel matrix. The solution was then bath sonicated for 20 minutes to break apart any remaining aggregates. The resulting solution was semi clear and homogenous.

*2.4.8 SWNT concentration of hydrogels*

SWNT sensors were crashed out of the hydrogel solution using 1 M HCl to remove ssDNA wrapping surrounding the carbon nanotubes. The unwrapped SWNT began to form clumps due to the hydrophobic nature of the nanotubes. The solutions were neutralized using 1 M NaOH and a pH meter to allow for the formation of SWNT pellets. The solutions were centrifuged for 180 minutes (16,100 RCF) and the supernatant was removed leaving behind a SWNT pellet. Nanopure water was added to the SWNT pellets along with tip sonication (5W) followed by centrifugation. The washing step was repeated three times to remove any remaining HCl/NaOH. Following washing step SWNT was resuspended using $(AT)_{15}$ as described previously. Resulting SWNT solutions were analyzed using UV/Vis spectroscopy to obtain concentrations.

*2.4.9 Biodistribution of SWNT*

Tissues were degraded using a similar process to hydrogel degradation. The tissues were frozen at -20 C and 1 mL of tissue was dissected and homogenized using a sharp blade (the process was repeated three times for each tissue using different areas). The resulting homogenate was suspended in 3 mL of HCl to remove the ssDNA wrapping on the carbon nanotubes. The nanotubes began to crash out of solution and NaOH was added dropwise under the supervision of a pH meter to bring the solution to neutral pH. The solution was then centrifuged (16,100 RCF) for 180 minutes and the supernatant was removed. The containers were then washed three times using nanopure water, tip sonication, and centrifugation. Finally, ssDNA was added to the containers and the wrapping procedure for SWNT was followed. The spectra were then obtained using Raman spectroscopy.

Briefly, a Renishaw inVia Raman microscope was used to collect sample spectra from 190 to 3500 nm. Samples were loaded into capillary tubes and placed on the microscope stage and a 20X objective was used to collect the signal. SWNT standard solutions and artificially added SWNT that had been extracted from clean tissue were analyzed to form concentration curves. Extracts from tissue homogenates were analyzed in the same way.

## 2.5 Results

### *2.5.1 SWNT retention by hydrogels.*

SWNT sensors for nitric oxide (NO) were fabricated and quantified using UV/Vis absorbance values that have previously been shown to accurately quantify SWNT. SWNT wrapped with $(AT)_{15}$ ssDNA have been shown to predictably respond with a fluorescence attenuation in the presence of NO, with little to no response to the presence of similar analytes (Figure 2-1a). The sensors were incorporated into an alginate hydrogel platform and fluorescence imaging at 990 nm (the characteristic emission wavelength of the 6,5 chirality SWNT) shows successful noncovalent suspension of the sensors (Figure 2-1b). Following fabrication, hydrogel sensors were implanted subcutaneously into the ears of 14 wether (<1 year old, castrated male) sheep under the supervision of a trained veterinarian (Figure 2-1c). Three weeks later the animals were sacrificed and tissues, along with the hydrogels, were harvested. The tissues and hydrogels were then assayed for SWNT content using the newly developed SWNT extraction methods.

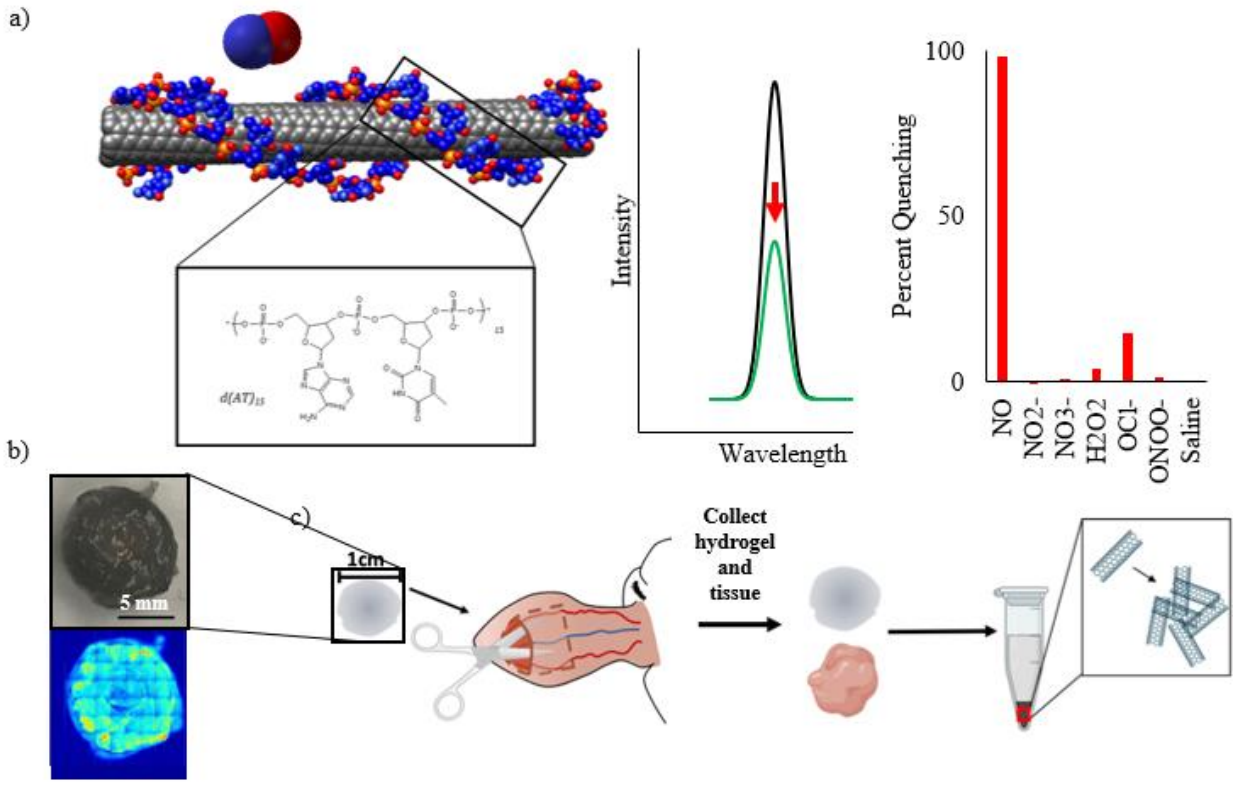


Figure 2-1: Overview of the sensor delivery procedure**.** (a) SWNT wrapped with $(AT)_{15}$ act as sensors of NO through fluorescent signal quenching, which occurs when the SWNT is exposed to NO, but does not occur when exposed to other analytes [58, 61]. (b) Representative brightfield and fluorescent (990 nm) images show that SWNT sensors were incorporated into alginate hydrogels while maintaining their fluorescent properties[112, 145]. (c) SWNT loaded hydrogels were placed within an animal, monitored for 3 weeks, removed from the animal, and analyzed to determine sensor retention and tissue accumulation.

To determine nanoparticle retention by the hydrogels a new method for SWNT extraction needed to be developed (Figure 2-2a). The hydrogels were digested using alginate lyase to release the SWNT sensors from the alginate matrix, leaving them suspended in a complex solution. To remove the SWNT from the degraded hydrogel components, the DNA wrapping was removed to take advantage of the hydrophobic nature of the nanotubes. DNA removal from the SWNT was performed through the

addition of 1 M HCl, causing the hydrophobic SWNT to aggregate. This was followed by the dropwise addition of 1 M NaOH to neutralize the solution. The solution was then centrifuged to create a SWNT pellet that is separate from the hydrogel components. The pellet was then resuspended by wrapping with DNA in normal saline and quantified through UV/Vis and Raman spectroscopy.

UV/Vis spectroscopy is the accepted method of quantification for freshly wrapped SWNT sensors, with the absorbance value of the sensors at the 632 nm valley used to calculate SWNT concentration[58]. Unfortunately, when SWNT is removed from the hydrogels, the 632 nm value is obstructed by absorbance from residual hydrogel components, which can be seen when comparing a SWNT solution with and without degraded hydrogel components. A solution of 5 mg $L^{-1}$ SWNT sensors with degraded hydrogel components appears to have a concentration similar to a clean 10 mg $L^{-1}$ SWNT sensor solution when using the 632 nm value. We determined that the 990 nm value can be used instead of the 632 nm value to quantify the solution, as it is in a portion of the spectrum that experiences less interference from the hydrogel components. When comparing the 5 mg $L^{-1}$ SWNT sensor solution that is with degraded hydrogel components to a clean 5 mg $L^{-1}$ SWNT sensor solution, the 990 nm values match (Figure 2-2b). This comparison of SWNT concentrations using the 990 nm value was performed on numerous concentrations of SWNT and was found to remain consistent (Figure 2-2 c,d).

To ensure NO exposure from the *in vivo* implantation did not alter measured UV/Vis spectra, SWNT solutions were exposed to NO and assayed to determine if their 990 nm value was altered (Figure 2-2e). The addition of NO did not alter the UV/Vis

spectra or the concentration curve, indicating *in vivo* NO exposure will not alter the ability to quantify the SWNT within the hydrogels.

As a secondary method of SWNT concentration analysis, samples were analyzed with Raman spectroscopy. The standard method of SWNT quantification, analysis of the G peak, was used to create a concentration curve of the SWNT after removal from hydrogels, again comparing it to clean SWNT and SWNT exposed to NO (Figure 2-2f). All three samples resulted in similar concentration curves relating the G peak intensity to SWNT concentration for SWNT ranging from 1 mg $L^{-1}$ to 10 mg $L^{-1}$.

Hydrogels that were extracted from the sheep's ears following 21 days post implantation were analyzed using this new extraction process and were assayed for concentration using UV/Vis and Raman spectroscopy (Figure 2-2g). SWNT-Alginate hydrogels that were originally made with 10 mg $L^{-1}$ SWNT contained 8.9 mg $L^{-1}$ SWNT after removal from the sheep. The non-SWNT control gels resulted in a small, non-significant signal.

The observed decrease in SWNT concentration from the initial concentration when the hydrogels were implanted to the concentration post sacrifice is hypothesized to be due to the physical extraction of the hydrogels from the tissue. Handling and sacrifice of larger animals like sheep is less controlled than rodents in the laboratory setting, and it is possible that handling of the sheep led to tearing of the hydrogels *in vivo*. While the majority of the hydrogels were recovered and subject to the SWNT extraction process, it is possible small parts of the hydrogel were damaged during the sacrifice and hydrogel retrieval process and not recovered with the rest of the gel.

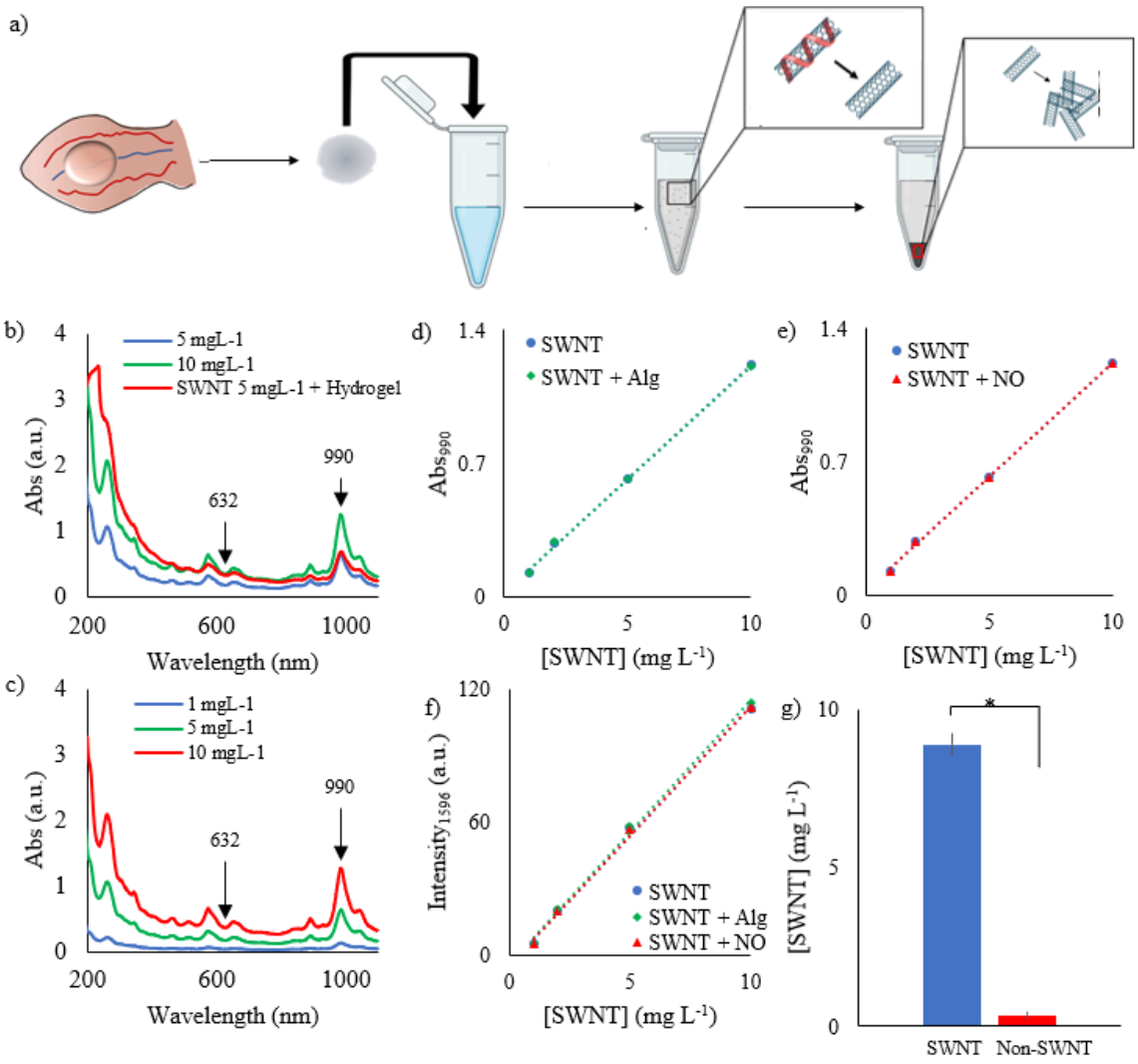


Figure 2-2: Extraction of nanoparticles from hydrogel platform. (a) A schematic depicting the novel SWNT extraction method shows the degradation of the hydrogels, the unwrapping of the SWNT and their isolation from the solution. (b) UV/Vis spectroscopy shows spectra of SWNT with degraded hydrogel components compared to clean SWNT solutions. Analysis of the widely used 632 nm value provides inaccurate quantification of the hydrogel associated SWNT, but the 990 nm value provides accurate quantification (means are shown; n= 3). (c, d) Various concentrations of SWNT spectra from the UV/Vis was collected to create a concentration curve correlating 990 nm value and SWNT concentration of clean and hydrogel associated nanoparticles (means are shown for c; means ± S.E. are shown for d; n= 3; P> 0.05; two-sided t-test, $R^2 > 0.99$). (e) Samples exposed to NO undergo fluorescence attenuation, but UV/Vis spectroscopy absorbance values were unaffected (means ± S.E. are shown; n= 3; P> 0.05; two-sided t-test, $R^2 > 0.99$). (f)

Raman spectroscopy served as a secondary method for quantification of SWNT extracted from the hydrogels by demonstrating that the G peak of hydrogel associate, clean and NO exposed SWNT did not differ (means ± S.E. are shown; n= 3; P> 0.05; one-way ANOVA, $R^2 > 0.99$). (g) Both methods of SWNT quantification were used to quantify the SWNT extracted from the implanted hydrogels. It was found that gels initially containing 10 mg $L^{-1}$ SWNT contained 8.9 mg $L^{-1}$ and the control, non-SWNT gels showed a non-significant signal (means ± S.E. are shown; n= 9; *P= 1 x $10^{-11}$; two-sided t-test).

### *2.5.2 Biodistribution of SWNT.*

As previously stated, SWNT aggregation in cells and tissues remains a concern when using SWNT-based sensors *in vivo*. Tissues were harvested from sheep 21 days post implantation in order to assess whether or not a detectable amount of SWNT had left the hydrogel platforms and aggregated in the tissue. The excised tissues were assayed for SWNT concentration following a similar extraction method to the extraction method used for the hydrogels (Figure 2-3a). The tissue was frozen, to allow for better homogenization, before being homogenized and placed in HCl, which degraded the tissue and remove the ssDNA wrapping from the SWNT. As shown in figure 2-2, the hydrogel platforms were successful in retaining the majority of the SWNT that they initially contained, so Raman spectroscopy, which is able to detect much lower concentrations of SWNT than UV/Vis (detection limit of approximately 0.3 mg $L^{-1}$), was used to analyze these samples. We were able to reproducibly detect concentrations of SWNT in solution as low as 0.03 mg $L^{-1}$ (Figure 2-3b), which is in accordance with previously published report on SWNT circulation and fate[137]. Control samples of tissue with varying concentrations of SWNT were subjected to the extraction protocol and a standard curve

was developed for both the SWNT solutions exposed to degraded tissue and the clean SWNT solutions (Figure 3c). We found that there is no significant difference in the Raman spectrum or values for the two types of samples (Figure 2-3c). Blood, heart, kidney, liver, lung, and pancreas tissue harvested from the sheep post-sacrifice were processed and analyzed as described above and it was found that there was no detectable concentration of SWNT in any of the samples (Figure 2-3d).

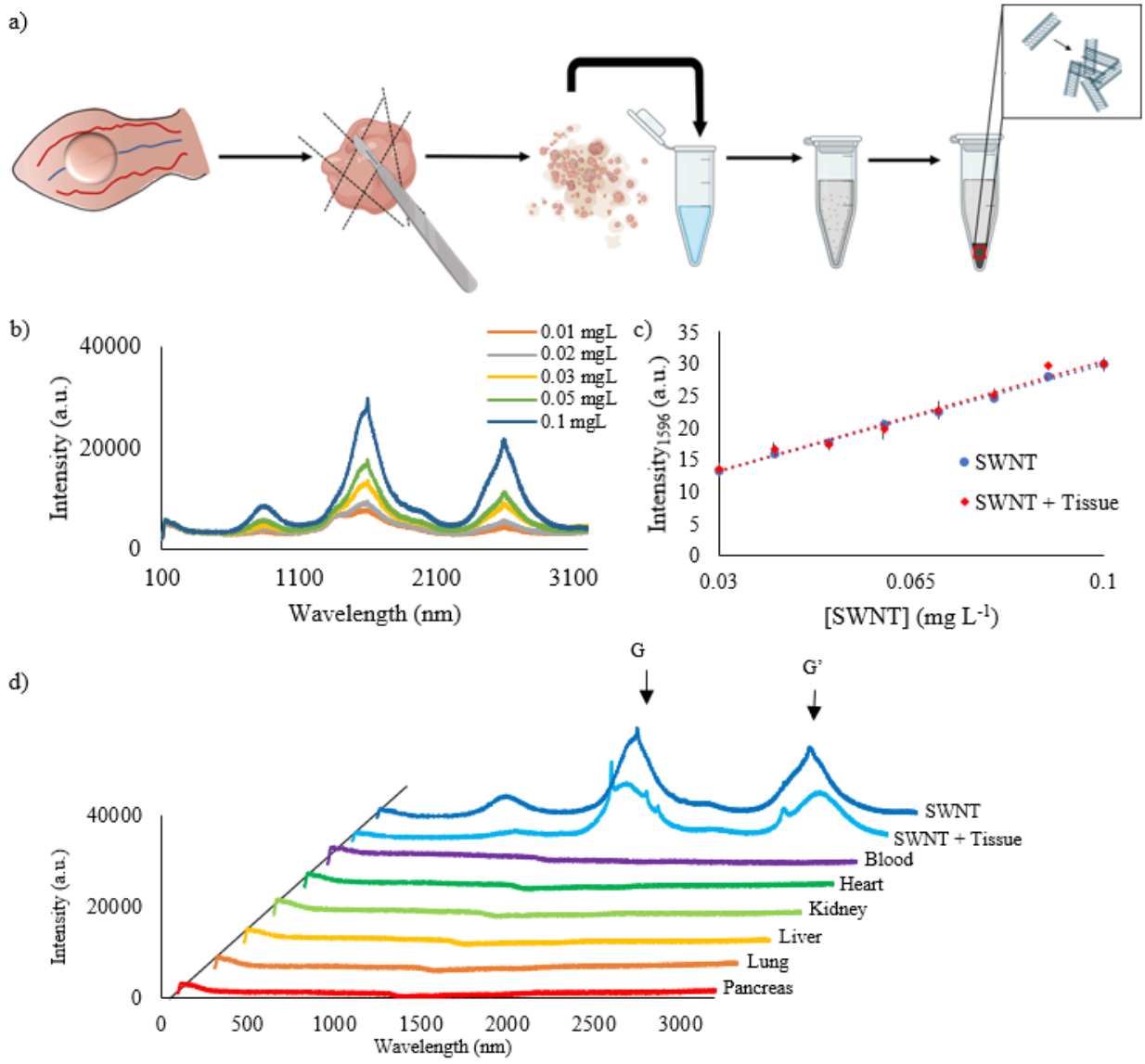

Figure 2-3: Determination of biodistribution of nanoparticles. (a) a schematic depicting the process for the extraction of SWNT from tissue. (b) Raman spectra for varying concentrations of SWNT show that there is a decrease in G peak values with a decrease in SWNT concentration, this data was used to create a concentration curve for SWNT in solution (blue dots/line in c) (means are shown; n= 3) (c) a concentration curve was developed to compare the detection of SWNT in solution (blue) and SWNT exposed to degraded tissue (red) using Raman spectroscopy (means ± S.E. are shown; n= 3; P> 0.05; two-sided t-test). (d) Harvested tissues were subjected to the SWNT extraction method and the resulting solutions were analyzed with Raman spectroscopy. No SWNT signal was detected for any of the tissue harvested from the animals (means are shown; n= 3).

## 2.6 Discussion

Fluorescent SWNT sensors provide unparalleled spatiotemporal resolution for biological analytes and are a promising new class of biosensors, but toxicity concerns have plagued the SWNT sensor field for years due to the unknown long-term risks associated with free SWNT being localized within various tissues[137]. By using a stable SWNT platform, it is possible to remove and replace implants as needed without concern of sensor leeching leading to SWNT accumulation and potential health hazards. This study was performed on animals that had hydrogels implanted for 21 days, but it is possible that even longer-term health monitoring could be performed with these platforms, since detection of *in vivo*, hydrogel encapsulated SWNT sensors has been shown for 300 days in previous studies [60].

Functionalized SWNT have been employed in numerous biological systems, especially in the last few years [73, 78, 79, 83, 85, 88, 97-99, 101], but a large animal study demonstrating SWNT retention has not been performed. One difficulty associated with large animal research is that the preferred method of minor surgical procedures, such

as subcutaneous implantations, is to have the animal conscious, leading to a wide range of issues that do not occur when working with anesthetized rodents. Other issues that may have impeded SWNT sensor testing in large animals in the past is the need for large animal housing, veterinary care, and sacrifice facilities. As one of the leaders in agriculture and animal research, the University of Nebraska has access to state-of-the-art facilities for large animal care, making this research possible for the first time.

The sheep model used in this study is advantageous to the highly used rodent models found in the literature because sheep more closely model humans. Not only are the physiology and genetics of sheep more similar to humans, but also the relative size of the animals is more similar to humans. Detection of fluorescent probes in rodents and in larger animals is mostly dependent on the detection scheme and the amounts of probe required for successful signal detection in either case is similar. Due to the dramatic difference in size of the two models, the relative concentrations of fluorescent probe to animal are drastically different between sheep and rodents. The sheep better model the "dose" of sensors that would be required for use in humans and allow insight into fate of SWNT sensors for larger animal systems.

The experiments performed here have shown that SWNT-hydrogel platforms are capable of retaining the majority of the initially incorporated nanoparticles and that there is no detectable aggregation of nanotubes present in key tissues. The hydrogel platforms used in this study can easily be adapted for use with SWNT sensors for alternate analytes and even for different types of nanoparticles. SWNT sensors for insulin, glucose, nitric oxide, dopamine, and specific RNA and DNA segments, [58, 59, 61, 65, 69, 71-73, 78, 83, 87, 100, 131, 135, 136] already exist, and SWNT sensors for other analytes are

currently being developed by multiple researchers, resulting in a large number of analytes that could potentially be monitored.

Translation of technologies to humans is always at the forefront of biomedical engineering. The methods developed in this research have an immediate impact on the SWNT sensor community as it allows researchers an avenue for measuring the fate of nanoparticles in a large animal, alleviating toxicity concerns and moving the sensors one step closer to clinical use. Localized SWNT sensors could eliminate the need for patient samples such as blood draws, as the SWNT sensors could provide real time measurements of various analytes in blood or specific tissues. In the future, SWNT sensors could be combined with wearable technology and provide early detection of biomarkers for many disease states as the only requirements for operation would be excitation and emission collection.

# CHAPTER 3

## Detection of Single Walled Carbon Nanotube Based Sensors in a Large Mammal

### 3.1 Abstract

High resolution, rapid, and precise detection of biological analytes related to disease and infection is currently the focus of many researchers. Better biosensors could lead to earlier detection, more avenues of intervention, and higher efficacy of therapeutics, which would lead to better outcomes for all patients. One class of biosensors, single walled carbon nanotubes, is unique due to their nanoscale resolution, single molecule sensitivity, and reversibility for long term applications. While these biosensors have been successful in rodent models, to date, no study has shown successful sensor detection in a large animal. In this study, we show the first successful signal detection of single walled carbon nanotube-based sensors in a large mammal model. Using a relatively simple and cost-effective system, we were able to detect signals in nearly 70% of the sheep used in the study, marking an important steppingstone towards the use of SWNT-based sensors for clinical diagnostics.

### 3.2 Introduction

Translation of biosensors capable of efficient, facile, and rapid testing of key analytes to clinical use has the opportunity to save lives and curb infection.[146] Single walled carbon nanotubes (SWNT) have seen an exponential rise in biosensing applications in recent years.[74, 89, 147-149] SWNT-based optical biosensors allow researchers to develop detection schemes with unparalleled spatial and temporal resolution, and highly

stable fluorescence in the near infrared (nIR) range allows for long term detection in a biological medium capable of single molecule detection.[61, 79, 82]

The outstanding optical properties of SWNT are due to the unique nature of their electronic structure.[44, 49, 127] Perturbation of dielectric environment along the one-dimensional carbon structures results in predictable fluorescence modulations.[76, 131, 134] Noncovalent functionalization of SWNT can control the observed fluorescence shifts to occur only in the presence of specific molecules.[66]

The SWNT sensor library is rapidly growing and now includes sensors for HIV, neurotransmitters, glucose, insulin, free radicals, ovarian cancer biomarkers, and many more key analytes.[78, 83, 100, 135, 150] Most recently, a SWNT-based sensor for the SARS-CoV-2 spike protein has been developed.[151] Long-term monitoring of these key biological analytes could provide important health information for better patient outcomes. To this end, *in vivo* monitoring via SWNT biosensors has been shown in mice for 300 days with no adverse effects.[112] However, translation to larger animal models has remained elusive to the community primarily because nanotechnology laboratories and equipment are not designed to house, handle, and monitor large animals.

In this study SWNT were functionalized with $d(AT)_{15}$ to create a sensor for nitric oxide (NO) before being incorporated into the matrix of alginate hydrogels. The sensor encapsulated hydrogels were subcutaneously implanted into the ears of 14 male sheep and detected with an nIR spectrometer and a noncoherent light source (Figure 3-1). Signal detection was shown in a large animal model for the first time using a simple, inexpensive setup and a small amount of sensor. These results are a key step towards clinical use of SWNT sensors.

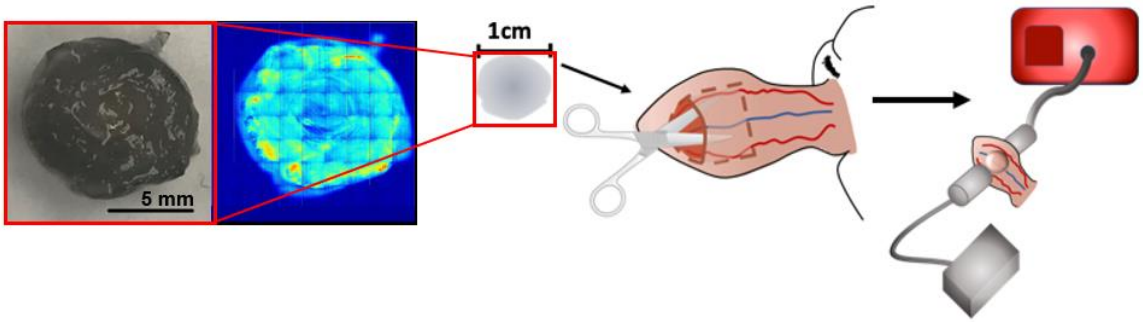


Figure 3-1: Study overview. SWNT sensors for nitric oxide were successfully incorporated into alginate hydrogels and a photograph next to a fluorescence image taken a 990 nm (the characteristic wavelength for 6,5 $AT_{15}$ SWNT sensors) can be seen. Fluorescence signal detection *in vivo* was accomplished using a noncoherent light source and a nIR spectrometer.

## 3.3 Animal Use

All animal protocols and handling were approved by the Institutional Animal Care and Use Committee at the University of Nebraska-Lincoln [Protocol No. 1751].

## 3.4 Methods

### *3.4.1 SWNT Sensor Fabrication*

Single wall carbon nanotubes were purchased from Sigma Aldrich ((6,5) chirality, 0.7-0.9 tube diameter, carbon <95%, >93% carbon as SWNT) and ssDNA (d(AT)15 oligo) was purchased from Integrated DNA Technologies (IDT). SWNT sensors were prepared according to previous experiments. In brief, SWNT was suspended in 1:2 mass ratio with ssDNA in normal saline. Resulting suspension was bath sonicated (Bransonic, M2800H) for 10 minutes to separate SWNT bundles followed by ultra-sonication with a

3 mm probe tip sonicator (QSonica Q125 Sonicator) for 40 min to disperse individual nanotubes. The solution was then centrifuged (Beckman Coulter Microfuge 16) for 180 min at 16100 RCF and to remove any unwrapped SWNT and the supernatant was collected. The resulting nanotube sensor suspension was then diluted 10fold and UV/vis spectrometry (Beckman Coulter DU730) was used to determine concentration as described previously.

### *3.4.2 SWNT/Alginate Hydrogel*

Alginate (Protanal RF 6650) was dissolved at 3% w/v in normal saline and SWNT sensor suspension was diluted to 30 mg L-1. The two solutions were mixed to create a final 2% alginate solution with 10 mg L-1 SWNT sensors. The resulting alginate-SWNT precursor solution was filled into a 10 mm diameter dialysis membrane (Fisherbrand, MWCO 3,500 d) to form a 10 cm long tube. The tube was then placed into a beaker containing 0.1 M CaCl2 for crosslinking. The precursor solution was allowed to crosslink for 24 hours in the calcium chloride solution. The tube hydrogel was removed from the dialysis membrane and cut into 3 mm thick discs. The hydrogels were stored in normal saline at room temperature prior to implantation.

### *3.4.3 Microscope Fluorescence Measurements*

A custom built nIR hyperspectral microscope (Photon Etc.) was used to obtain spectra for each individual pixel in the viewing window. In brief, an upright microscope

was modified with a 561 nm laser excitation source and an InGaAs camera array detector coupled with a volume Bragg grating to collect sample emission. Samples were placed under the 5x objective and excited with the 561 nm laser (~500 mW at the sample) and the resulting fluorescence was passed through a high pass filter to the volume Bragg grating where wavelength was specified. The InGaAs camera array collected the emission data and passed it on to the PhySpec software (Photon Etc.) where the signals were processed. All post processing of data cubes was done using MATLAB.

### *3.4.4 Quenching Experiments*

Nitric oxide gas was bubbled into deoxygenated saline by first bubbling argon gas through the solution using airtight caps and needles. Following deoxygenation, nitric oxide was bubbled slowly for 20 minutes and the resulting NO solution was assayed for concentration using horseradish peroxidase (HRP). The stock solution was then divided into deoxygenated flasks and, using deoxygenated saline, diluted to the concentrations used in experiments.

### *3.4.5 Spectrometer Fluorescence Detection*

An nIR spectrometer (B&W Tec) was used to collect average fluorescence intensity in the viewing window. A noncoherent light source (ThorLabs) was used to excite samples by using a liquid light guide fit with a lowpass (850 nm cutoff) filter to decrease noise. Sample emission was collected using a collimator connected to the nIR

spectrometer via fiber optic and the angle between the collector and light guide was 180 degrees unless otherwise specified.

### *3.4.6 In Vivo Study*

Wethers (<1 year old male sheep) were sheared, and a topical hair remover was used to clear implantation sites on ears. Under the supervision of trained veterinarians, local anesthetic was applied and subcutaneous implantation of the SWNT hydrogels was accomplished. Following a weeklong recovery period, animals were isolated using a trimming deck and the hydrogels were probed for signals using the nIR spectrometer and noncoherent light source.

## 3.5 Results

### *3.5.1 Microscope Characterization of Hydrogels*

SWNT sensors were encapsulated within alginate hydrogels that were then placed in the animal model. Previous research has shown that changes in hydrogel conformation can lead to changes in sensor function, so the newly developed SWNT-hydrogels needed to be characterized. Hyperspectral microscopy was used to quantify fluorescence intensity from the SWNT within the hydrogels. Figure 3-2 describes the fluorescent properties of SWNT/Alginate hydrogels versus SWNT alone and the fluorescence attenuation in the presence of the target analyte, nitric oxide (NO). Figure 3-2a shows the

incorporation of SWNT into alginate hydrogels (blue) does not significantly alter the fluorescence signal of the sensors when compared to SWNT alone (red). Comparison of the full width at half-maximum (FWHM) for the 990 nm peak reveals no significant difference between SWNT alone (28.6 nm) and SWNT/Alginate (28.2 nm). Figure 3-2b/3-2c show the response of SWNT sensors alone or incorporated into alginate have a similar response to the addition of the same concentration of NO. After confirming that the alginate was not interfering with the function of the sensors, a concentration curve was developed using the fluorescence quenching percentage versus NO concentration (Figure 3-2d). The response of the sensors to the addition of NO is dose dependent, with each concentration of NO resulting in a statistically different quenching response when compared to all other treatments ($n = 9$, $p < 0.05$).

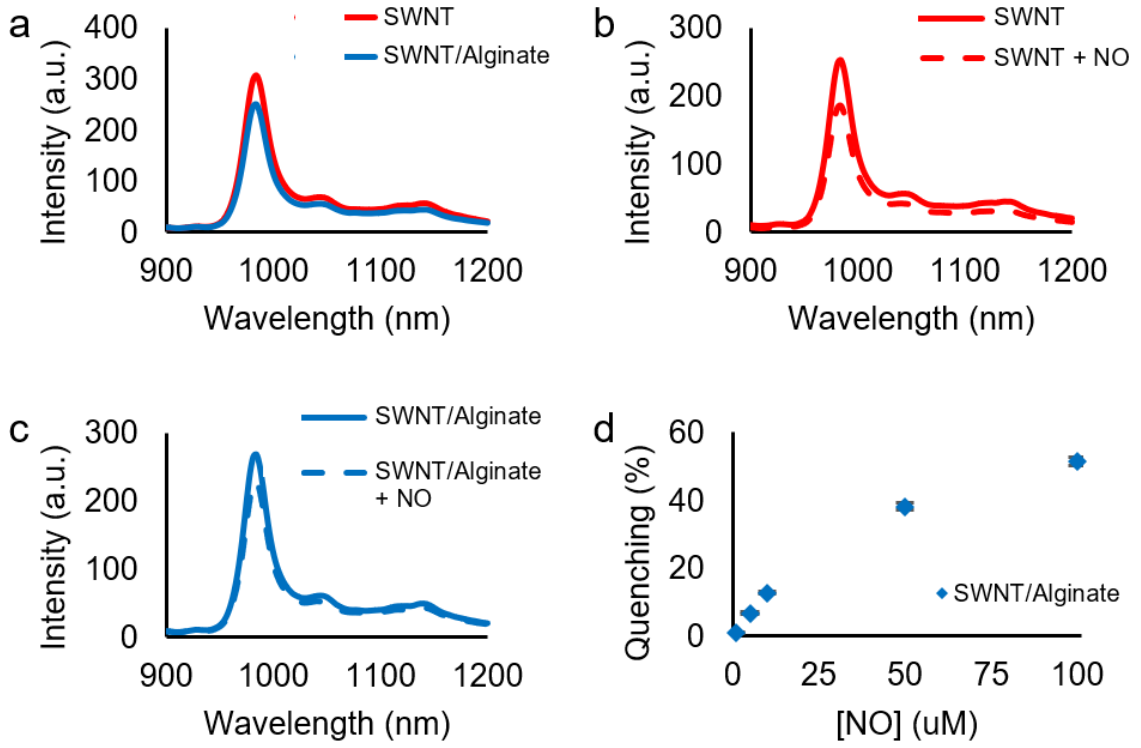


Figure 3-2: Fluorescence characteristics of SWNT hydrogels via hyperspectral microscope detection. SWNT sensors incorporated into alginate hydrogels do not experience a significant signal modulation and (a) spectra of free-floating SWNT sensors (red) (FWHM = 28.6 nm) and SWNT sensors incorporated into an alginate hydrogel (blue) (FWHM = 28.2 nm) shows little difference in signal intensity without shifting or changing peak location. SWNT sensors exposed to NO will experience fluorescence attenuation and (b) spectra of SWNT sensors (red) and SWNT sensors after adding NO (red dashed) shows a significant signal quenching. Incorporation of SWNT in alginate hydrogels does not alter sensor responsiveness to NO and (c) spectra of SWNT incorporated in alginate before (blue) and after NO addition (blue dashed) show a similar signal quenching the free-floating sensors. The response of SWNT sensors to NO is dose dependent as more analyte will cause a larger quench of the signal and (d) a plot of NO concentration versus percentage of signal quenched shows a direct relationship ($n = 9$, mean ± SEM, $p < 0.05$).

*3.5.2 Spectrometer Characterization of Hydrogels*

The hyperspectral setup is not portable and cannot accommodate large animals, therefore a more portable and versatile detection method had to be developed. Using a noncoherent light source and an nIR spectrometer, high-resolution, spectral detection of SWNT sensors can be accomplished. SWNT/Alginate hydrogel fluorescence properties were characterized using the setup and the results were compared to the hyperspectral microscope results. Figure 3-3a shows the comparison of SWNT alone (red) and SWNT/Alginate (blue) on both the microscope (solid lines) and on the large animal signal detection setup (dotted lines). The microscope uses a 561 nm laser for excitation which is the characteristic excitation wavelength of the 6,5 chirality of SWNT, whereas the spectrometer uses a noncoherent light source which excites over most visible wavelengths. Since purification by chirality is difficult, the samples used in this study were not composed entirely of 6,5 chirality SWNT and contained trace amounts of other SWNT chiralities. As the excitation source wavelength range is broadened, the SWNT of different chiralities were excited to a larger extent and contribute more to the overall spectra. Despite this change, the shape of the 6,5 chirality SWNT peak at 990 nm was not altered between setups. Since the function of the sensors relies solely on the 6,5 chirality fluorescence emission and this peak was not altered, the sensors function similarly between detection schemes. After validating the detection scheme a dose dependent concentration curve was developed using the SWNT/Alginate hydrogels and varying NO concentrations. Figure 3-3b shows a similar to the curve obtained from the microscope

setup (Figure 3-2d), with each NO concentration resulting in a statistically unique quenching response from all other treatments ($n=9$, $p<0.05$).

### *3.5.3 In Vivo Parameters*

In order to ensure the highest intensity fluorescence *in vivo* without causing harm to the animals, the light source power was optimized. A tissue phantom (sheep ear) was used to determine the highest possible light source intensity and exposure time that could be used in the study without irritating the skin. Figure 3-3c shows the results of varying the two parameters with a "+" indicating signs of skin irritation, and a "-" indicating no skin irritation. The highest light source power that resulted in no irritation was 75% at 1 second exposure time which is compared to the signal collected at 100% power and 1 second exposure time in figure 3-3d. The signal is decreased using the lower power, but it the intensity still allows for signal detection.

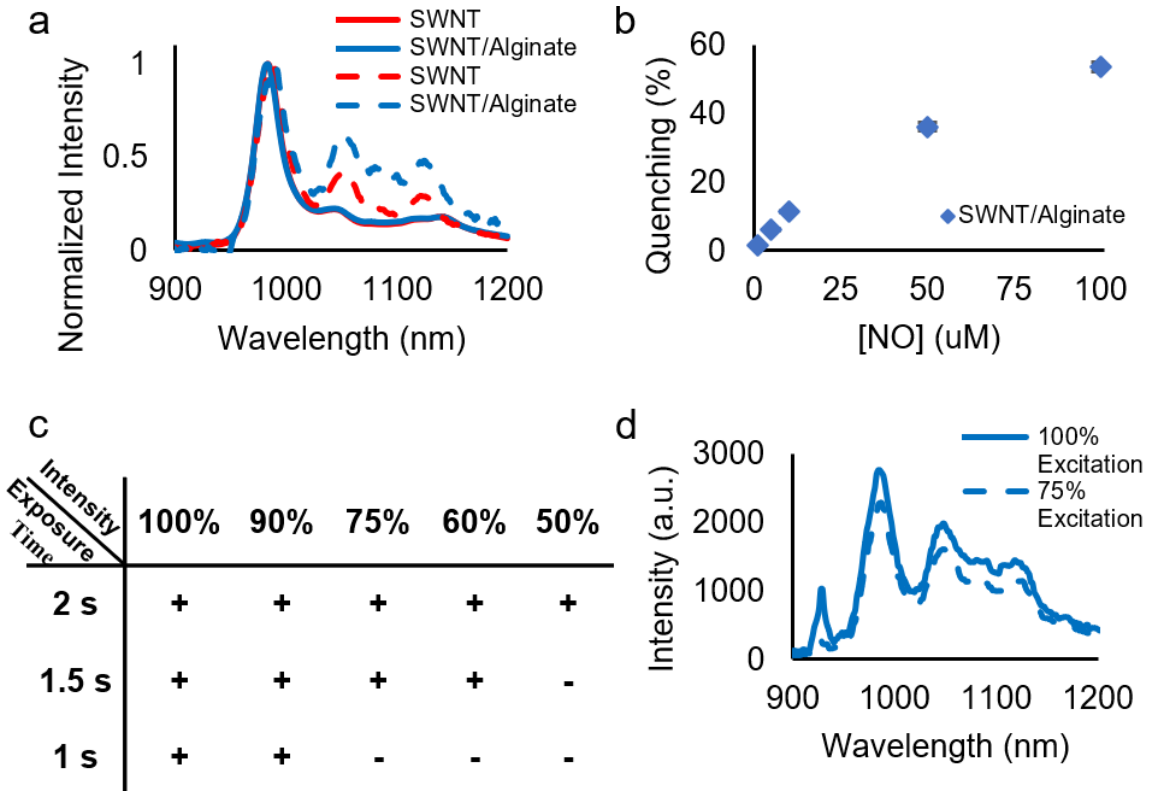


Figure 3-3: Detection method validation. In order to validate the newly employed detection scheme for the *in vivo* experiment, comparison to the previously published method of detection was performed. Free floating SWNT sensor signals (red) (a) were compared to SWNT incorporated in alginate hydrogel signals (blue) for both the hyperspectral microscope (solid) and the spectrometer (dashed). The SWNT hydrogel signal was probed for response to NO (b) and showed a similar quenching response to the microscope (n = 9, mean ± SEM, $p < 0.05$). The light source intensity (c) was adjusted to optimize signal without damaging skin and spectra (d) for the optimized light source intensity was compared to the maximum intensity.

### *3.5.4 In Vivo Detection*

Tissue phantoms (sheep ears) were used to show successful detection of SWNT/Alginate hydrogels *in situ* and NO was added to the phantoms to ensure that sensor function was not unaltered. In Figure 3-4a, images at 990 nm are displayed next to

a photograph of an implanted SWNT/Alginate hydrogel showing fluorescence from the gel when compared to background tissue. After confirmation of gel detection *in situ,* a dose dependent concentration curve was collected for NO in the tissue phantoms, once again showing a statistically unique quenching response to each NO concentration when compared to all others (Figure 3-4b, $n=9$, $p<0.05$). The concentration curve is similar to the two previously collected curves for the SWNT/Alginate hydrogels in saline with the microscope and the spectrometer (Figures 3-2d and 3-3b): however, the quenching responses for each concentration are slightly decreased *in situ*. The quenching experiments in Figures 3-2 and 3-3 were accomplished using well plates with precisely defined volumes, whereas the *in situ* experiments were performed in subcutaneous pockets of less controlled volumes. After showing the signal and detection properties of the SWNT/Alginate hydrogels was unaffected by implantation in sheep ears *ex vivo,* the sensors were analyzed *in vivo*. SWNT/Alginate hydrogels were implanted into the ears of 14 wether (<1 year old, castrated) sheep. Following one week of recovery the sheep were individually moved from their pens and restrained on a trim stand. Signals were detected for 9 of the 14 animals used in this study and Figure 3-4c shows a representative spectrum of the detected signals. It is interesting to note the 6,5 chirality peak at 990 nm appears to be attenuated compared to signals collected in the lab (using the other chirality peaks as a reference), and it is hypothesized this attenuation is due to endogenous NO. Detection of the SWNT/Alginate hydrogels in this study marks the first successful *in vivo* detection of SWNT signals in a large animal.

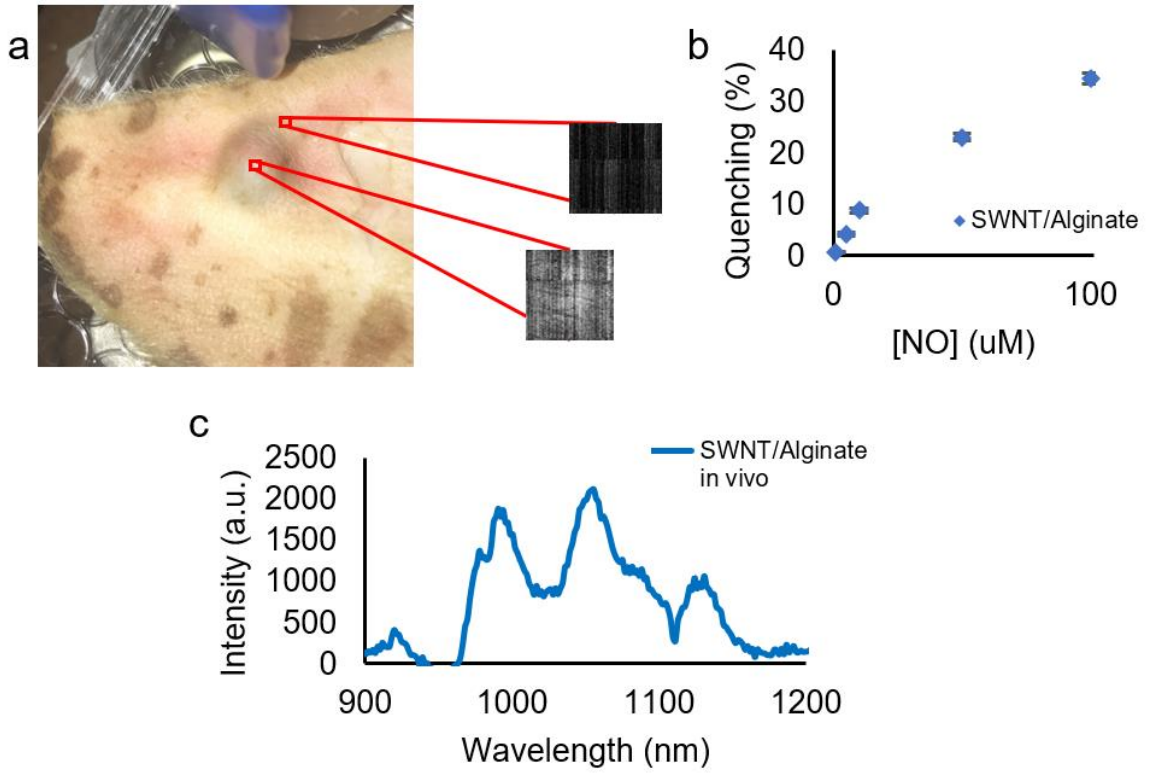


Figure 3-4: *In vivo* detection. SWNT/Alginate hydrogels (a) were implanted into ear phantoms and a photograph is displayed next to a fluorescent image at 990 nm showing successful detection. The SWNT/Alginate hydrogel response to NO (b) was probed and found to show a similar dose dependent sensor response to NO concentration (n = 9, mean ± SEM, $p < 0.05$). Animals received SWNT hydrogel implants and following a healing period the gels were probed for SWNT fluorescence. The spectrum in c is a representative spectrum of the signals that were detected in 9 of the 14 animals used in this study.

### 3.6 Discussion

The data presented in this study marks the first successful detection of a SWNT sensor signal in a large animal. It is an important step towards the use of the versatile and powerful sensors in humans. Signal detection was accomplished using a simple detection scheme of a noncoherent light source and an nIR spectrometer, both of which are relatively inexpensive, have a small footprint, and can be easily transported to the

location of the animal. The amount of SWNT needed to obtain a signal in the large animal was very small compared to the size of the animal, with 89% of the SWNT retained in the hydrogels over a 21-day period, mitigating concerns of possible long-term toxicity.[152] Sensor signal remained detectable even at low light source intensities and further optimization of excitation light to a narrower bandwidth could allow for higher fluorescence intensity values with less concern of skin irritation. As the world is becoming more focused on the need for continuous sensing, the placement of the SWNT sensor into a large animal model is an important step towards the translation of this technology in humans.

# CHAPTER 4

## Implantable Nanotube Sensor Platform for Rapid Analyte Detection

### 4.1 Abstract

The use of nanoparticles within living systems is a growing field, but the long-term effects of introducing nanoparticles to a biological system are unknown. If nanoparticles remain localized after *in vivo* implantation unanticipated side effects due to unknown biodistribution can be avoided. Unfortunately, stabilization and retention of nanoparticles frequently alters their function.[153] In this work multiple hydrogel platforms are developed to look at long term localization of nanoparticle sensors with the goal of developing a sensor platform that will stabilize and localize the nanoparticles without altering their function. Two different hydrogel platforms are presented, one with a liquid core of sensors and another with sensors decorating the hydrogel's exterior, that are capable of localizing the nanoparticles without inhibiting their function. With the use of these new hydrogel platforms nanoparticle sensors can be easily implanted *in vivo* and utilized without concerns of nanoparticle impact on the animal.

### 4.2 Introduction

Nanoparticles are attractive sensors for *in vivo* research due to their small size and large variability in sensing capabilities. Single wall carbon nanotube (SWNT) sensors are of particular interest for *in vivo* research due to their photostability, emission wavelength and biocompatibility.[51-53, 154] SWNT have been shown to maintain their fluorescent signal over an extended period of time despite exposure to light,[134] fluoresce in the

near infrared (nIR) region, where minimal light is absorbed by blood and water,[49] and be biocompatible for both *in vitro* and *in vivo* applications.[137, 155-164]

Despite their many advantages, there are drawbacks in the use of SWNT *in vivo*. One complication for SWNT sensors is that fluorescent signals lose intensity as they travel through multiple layers of cells/tissue.[165] Another complicating factor is that due to their small size, SWNT sensors that are placed subcutaneously will diffuse away from the region of interest. The diffusion of the subcutaneous sensors occurs in a non-uniform, non-reproducible manner, making them difficult to use for long-term detection. Because of these limiting factors, the localization of SWNT sensors to a deliverable and implantable platform is required to improve long term sensing capabilities.

Hydrogels have been shown to be biocompatible, maintain stability, and allow light penetration, making them ideal candidates for a sensor delivery platform.[157, 165-168] An alginate hydrogel was developed to localize $(AAAT)_7$ wrapped SWNT (a nitric oxide sensor) in a mouse model and was shown to be stable for 300 days following subcutaneous implantation.[157] The encapsulation of the sensor within the hydrogel did not change the specificity of the sensor, but it did alter the rate of detection and recovery.[157] It is hypothesized that the rate change occurred due to interactions of the SWNT's single-stranded DNA (ssDNA) wrapping with the gel matrix. In this paper we will utilize new methods for SWNT sensor stabilization to determine which of these factors is responsible for altering sensing rates while developing a biocompatible, implantable system to localize nanoparticles without altering their intrinsic properties.

## 4.3 Methods

### *4.3.1 $(AT)_{15}$ Wrapped SWNT*

SWNT purchased from Sigma Aldrich ((6,5) chirality, 0.7-0.9 tube diameter, carbon <95 %, >93% carbon as SWNT) was suspended with a $d(AT)_{15}$ or a biotin-modified $d(AT)_{15}$ sequence of ssDNA (Integrated DNA Technologies) using previously developed methods.[150, 153] Briefly, SWNT and ssDNA were added in a 2:1 DNA:SWNT mass ratio to NaCl in nanopure water (0.1 M) (normal saline). The suspension was sonicated for 20 minutes with a bath sonicator (Bransonic, M2800H) followed by ultrasonication with a 3 mm probe tip sonicator (QSonica Q125 Sonicator) for 40 minutes. Suspension was centrifuged (Beckman Coulter Microfuge 16) for 180 min at 16,100 RCF and the supernatant was collected and stored at 4 C. Concentration of the SWNT-ssDNA solution was obtained via UV-Vis (Beckman Coulter, DU 730) and diluted with normal saline to obtain experimental concentrations.[150]

### *4.3.2 Fabrication of Alginate/SWNT Composite Hydrogel (AC)*

SWNT sensors were encapsulated within alginate as previously described.[120, 153] Briefly, $d(AT)_{15}$–SWNT suspension (10 mg $L^{-1}$) was added to alginate (Nova-Matrix, PRONOVA SLM 20, 3% w/v) to form a final 2% w/v alginate solution. Alginate-SWNT suspension was crosslinked by $BaCl_2$ in nanopure water (0.1 M) ($BaCl_2$

solution) in dialysis tubes (Thermo Scientific, Slide-A-Lyzer 2000 MWCO). Hydrogels were stored in normal saline at 37 °C.

### *4.3.3 Fabrication of Alginate Liquid-Core Hydrogel (ALC)*

SWNT sensor solution was encapsulated in alginate (Nova-Matrix, PRONOVA SLM 20) using three square molds (Stratasys Objet500 3D printer, material: RGD450) (see Supplemental figure 4-6). SWNT-ssDNA (30 mg $L^{-1}$) was deposited into mold 1 and frozen at -80 C. $BaCl_2$ was deposited into mold 2 and frozen at -80 °C to form two $BaCl_2$ halves. Frozen SWNT was placed between $BaCl_2$ halves and stored at -80 °C. Mold 3 was partially filled with 2% w/v alginate and SWNT-$BaCl_2$ core was placed on top of the alginate. Mold 3 was filled with 2% w/v alginate and crosslinked in a $BaCl_2$ bath. Hydrogels were either unaltered or trimmed to 8 mm x 8 mm x 8 mm. Hydrogels were stored in normal saline at 37 °C.

### *4.3.4 Fabrication of Hyaluronic Acid Liquid-Core Hydrogel (HALC)*

SWNT sensor solution was encapsulated with methacrylated hyaluronic acid (HA) via extrusion printing (EnvisionTec, 3D-Bioplotter). HA and gelatin (Nova-Matrix, Pharma grade 80, Sigma-Aldrich, Gelatin from bovine skin) were dissolved separately at 5% w/v in phosphate buffered saline (PBS). Methacrylic anhydride was added to HA and gelatin solutions and allowed to react for 6- and 1-hour periods, respectively. Resulting solutions were dialyzed against nanopure $H_2O$ for 3 days and solutions were lyophilized.

Hydrogel precursor solution was prepared by dissolving methacrylated HA and methacrylated gelatin at 5% w/v in $H_2O$ and adding a photoiniator at 0.5% w/v to induce crosslinking of polymer strands. A 1x1cm square containing a square compartment was developed with CAD (Autodesk, AutoCAD) and imported to the Bioplotter. Hyaluronic acid was loaded into the bioplotter extrusion head and the design was printed with UV crosslinking during a 30 second pausing after every second layer. After formation of the compartment, but before the top of the hydrogel was printed, a frozen SWNT solution (10 mg $L^{-1}$) square was deposited into the void. Solution was frozen in order to provide structural support for final two layers prior to crosslinking. After the final two layers of HA were deposited on top of the compartment, the entire hydrogel was crosslinked with UV light for 60 minutes. An identical procedure was followed for a second design consisting of a 1 cm x 1 cm square with two smaller rectangular compartments. Hydrogels were stored in normal saline at 37 °C.

### *4.3.5 Fabrication of Surface-Tethered Alginate Hydrogel (STA)*

A previously published procedure by Sultzbaugh and Speaker[169] was altered to tether the SWNT sensors externally to an alginate gel. Alginate was crosslinked for 24 hours with spermine (1% w/v) in HCl solution (0.2 M) (Sigma-Aldrich) using dialysis tubes (Thermo Scientific, Slide-A-Lyzer 2000 MWCO). Hydrogels were placed in an EDC/NHSS/Avidin (Sigma-Aldrich, N-(3-Dimethylaminopropyl)-N'-ethylcarbodiimide, N-Hydroxysuccinimide, Avidin from egg white, 4 μM) bath for 16 hours at 37 °C followed by a 16 hour biotinylated SWNT-d$(AT)_{15}$ (10 mg $L^{-1}$) bath at 37 °C. Ratios of

1:0, 2:1, and 1:1 biotin-modified $d(AT)_{15}$ to $d(AT)_{15}$ were used for the SWNT bath. Hydrogels were stored in normal saline at 37 °C.

### *4.3.6 Hydrogel Stability*

Hydrogel/sensor complexes were tested for stability by measuring size, sensor leaching, and fluorescence intensity at 990 nm. At days 0, 7, 14, 28, and 56 the normal saline bath in which the hydrogels were incubated was removed and analyzed via UV-Vis (Beckman Coulter, DU 730) to find the concentration of all SWNT, either fluorescent or non-fluorescent, in the solution.[150] An electronic caliper (Fisher Scientific, Traceable digital caliper) was used to precisely measure the dimensions of the hydrogels. Images of hydrogel platforms were captured to determine largescale physical degradation. Fluorescence intensity of the hydrogel/SWNT complex was determined using a custom-built near IR (nIR) hyperspectral microscope, similar to a previously developed system.[170] Briefly, samples were excited by a 561 nm laser, emission passed twice through a volume Bragg grating to reduce bandwidth and specify wavelength, and intensity was recorded pixel-by-pixel with an InGaAs camera (Xenics, Xeva-1.7-320 TE3).

### *4.3.7 Sensor Response to Analyte*

Sensitivity and reactivity of the hydrogel sensors to an analyte was determined using the custom-built nIR microscope. NO solution was created by bubbling gas through

an oxygen free, gastight flask containing normal saline and concentration was determined by electrochemical probe. Resulting NO solution was diluted to 600 μM in preparation for addition to sensing platforms. NO solution was delivered (10% v/v, final concentration of 60 μM) to each sample via gastight syringe and distance between injection and hydrogel was kept consistent. The fluorescence was continuously monitored for 10 minutes at 5 frames per second. An in-house developed program was used to analyze sample intensity over time. Sensitivity of each new hydrogel platform was compared to the previously employed AC hydrogels and free floating $(AT)_{15}$-SWNT in normal saline (FF SWNT) (10mg $L^{-1}$) to determine effectiveness of platform design on reactivity of sensors to the target analyte.

## 4.4 Results and Discussion

### *4.4.1 Hydrogel Sensor Development*

The three new hydrogel platforms, along with the previously developed alginate composite hydrogel (AC), were fabricated and observed for changes in size and fluorescence intensity (a schematic of hydrogel fabrication is presented in Supplementary figure 4-7). Figure 4-1 (a-d) shows representative images of the four types of sensor platforms with an accompanying image showing the SWNT intensity. The SWNT fluorescence images were recorded across the nIR spectrum, but only the intensity at 990 nm, the characteristic fluorescence wavelength for 6,5 SWNT, was extracted and displayed (for full spectra see Supplementary figure 4-8). The 990 nm images allow

conclusions about the homogeneity of SWNT distribution within each hydrogel to be drawn by highlighting major differences in fluorescence intensity, a more even color throughout the image indicates even SWNT distribution whereas appearance of dark red color indicates high aggregation of sensors compared to the hydrogel as a whole. AC (Figure 4-1a) and surface-tethered alginate hydrogels (STA) (Figure 4-1d) display 990 nm fluorescence evenly across the gel, while alginate liquid-core (ALC) (Figure 4-1c) and hyaluronic acid liquid-core (HALC) (Figure 4-1b) hydrogels show 990 nm fluorescence localized to central compartments. Emission at 990 nm indicates SWNT sensors were successfully incorporated in each hydrogel platform.

The ALC hydrogels exhibit a non-uniformity in SWNT dispersion, indicated by the dark red spot in the core, whereas the other three gels repeatedly demonstrate even SWNT fluorescence intensity throughout the region of interest. Because of the lack of uniformity and reproducibility the ALC hydrogels are not ideal for future *in vivo* use.

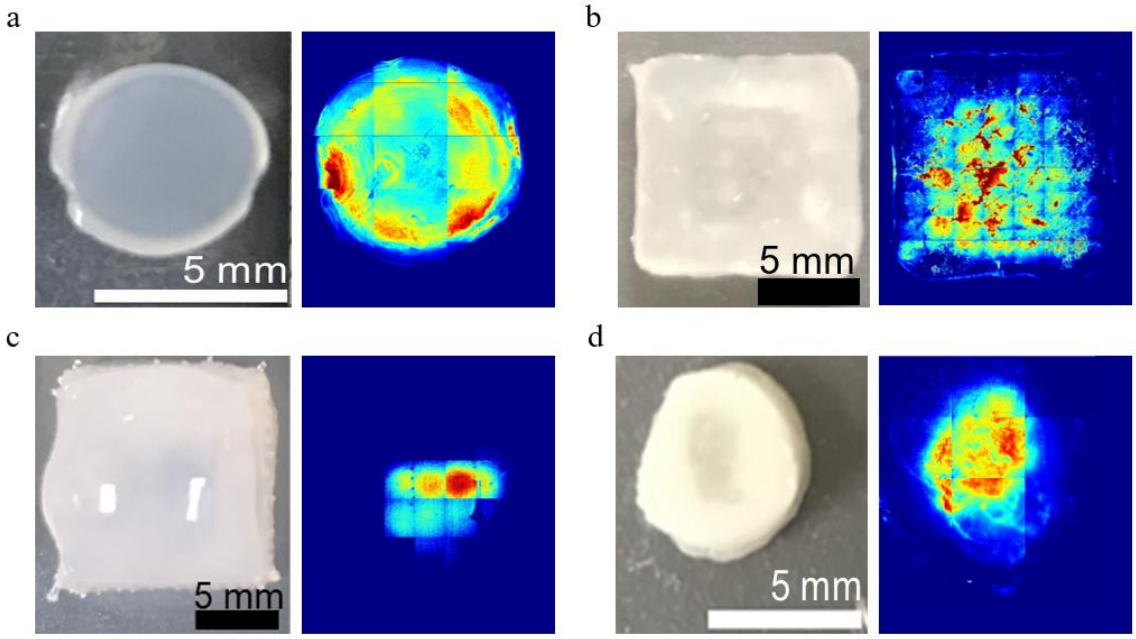


Figure 4-1: Representative photographs of the four types of hydrogel-SWNT sensor platforms with accompanying fluorescence image at 990 nm. Images depicting fluorescence intensity of the SWNT sensors are shown with red representing the highest intensity and blue representing the lowest intensity normalized to each image. Fluorescence images confirm association of SWNT sensors into hydrogel platforms. a) Alginate composite: AC, hydrogels show intensity spread across the entirety of the gel; b) hyaluronic acid liquid-core: HALC hydrogels show an even distribution of intensity within the core and little to no fluorescence outside of the core (edges); c) alginate liquid-core: ALC hydrogels did show fluorescence only within the core, but fluorescence is not well distributed; and d) surface-tethered alginate: STA hydrogels show and even distribution of fluorescence across the gel.

### *4.4.2 Hydrogel Sensor Stability*

The AC hydrogel has previously been shown to maintain its stability when implanted subcutaneously in a mouse model for 300 days.[153] In an attempt to avoid 300 day *in vivo* studies for all of the new hydrogel platforms, the new complexes were

compared to the AC hydrogel *in vitro*. Hydrogels were stored in normal saline (0.1 M NaCl) at 37 C to mimic *in vivo* conditions throughout stability testing. Measurement of hydrogel width and thicknesses showed no significant difference between the AC gels and the other delivery platforms except for day 14 ($p<0.05$ with one-way ANOVA), for which the AC gel showed an increase in size (Figure 4-2a). Swelling of hydrogels following the removal of chemical cross-linking agents is a common phenomenon,[171-173] and is believed to be the reason for the observed increase in gel size. The STA and the liquid-core hydrogels displayed less swelling than the AC hydrogel, presumably due to the different crosslinking agent and ability of the gel to swell inwards as well as outwards with the presence or absence of a liquid core, respectively.

Despite physical stability of the hydrogel-sensor complex, the fluorescence intensity of the sensors within the hydrogels decreased over the 56-day period (Figure 4-2b). In an attempt to determine whether the fluorescent signal decrease was due to a loss of nanoparticles, the storage saline of the hydrogels was tested for the presence of either fluorescent or non-fluorescent SWNT using a method previously shown by Attal et al. in which the absorption of the solution at 632 nm is used to quantify total SWNT concentration.[174] The concentration of SWNT within the storage saline was non-detectable. We propose that the decrease of SWNT fluorescence was a result of sensors leeching out of the hydrogels at a rate that was well under the detection limit of UV-vis spectroscopy, leading to a significant retention of fluorescence over the course of 56 days.

All four hydrogel platforms showed similar changes in SWNT fluorescence over time, leading to the hypothesis that the three new SWNT delivery platforms will show similar *in vivo* longevity as the previously tested AC platform.

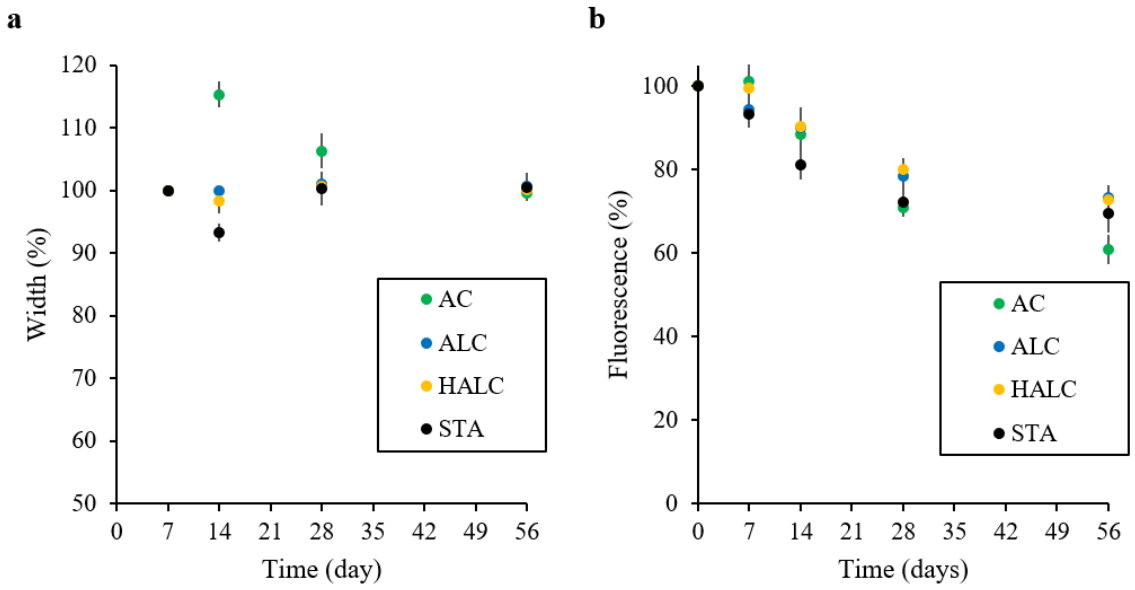


Figure 4-2: Stability of the hydrogel platforms were assayed at 7, 14, 28 and 56 days post synthesis through measurement of a) hydrogel width and b) sensor fluorescence normalized to initial values. AC hydrogels show significant swelling at day 14 ($p<0.05$). All hydrogel platforms show a significant decrease in fluorescence intensity from the initial value starting at day 28 ($p<0.05$), but no platform decreased significantly more than the others ($p>0.05$). (n = 3, error bars are s.e.m)

### *4.4.3 Analyte Reaction Rate*

Free-floating SWNT sensors (FF SWNT) in saline and all hydrogel sensor platforms were exposed to the target analyte and the fluorescence at 990 nm was recorded for a 10-minute period (Figure 4-3a). The SWNT sensors in this study are turnoff sensors, the fluorescence is expected to decrease in response to the addition of a target analyte.

Percent fluorescence is utilized to compare the fluorescence intensity of the gels since incorporation of the SWNT with the different gels leads to different levels of signal attenuation, specifically the internal vs external SWNT will receive different levels of excitation and have different lengths of wavelength paths for emission signal detection. As previously shown, the FF SWNT fluorescence was quenched rapidly in the presence of the target analyte, quenching 99.9% of the initial fluorescence intensity.[150, 175] The fluorescence of the HALC and STA hydrogels reacted similarly to the target analyte, quenching 99.9% and 97.3% respectively. AC and ALC hydrogels fluorescence quenched to a lesser extent, only quenching 95.3% and 80.2% within the 10-minute time period ($p<0.05$). The time to reach steady state for the SWNT in solution, HALC, and STA hydrogels were comparable, reaching steady state within 30 seconds of analyte exposure ($p>0.05$). The AC and ALC hydrogels had a significantly slower reaction rate, reaching steady state around 10 minutes and 8 minutes respectively ($p<0.05$). The maximum quenching value, time to ready steady state, and effective quenching rate of the platforms are compared in Table 4-1. As previously shown, the AC hydrogels decrease sensitivity of the SWNT to the target analyte and for both the AC and ALC hydrogels the maximum quenching value, time to reach steady state, and effective quenching rate are all significantly different ($p<0.05$) from the desired response of FF SWNT. HALC gels were not significantly different ($p>0.05$) from FF SWNT in any category, displaying a similar rapid response to the addition of the target analyte. STA gels did have a significantly different quenching rate from the FF SWNT ($p<0.05$), but the maximum quenching value and time to steady state were not significantly different from FF SWNT ($p>0.05$).

HALC hydrogels display similar quenching rates to the desired response of FF SWNT to addition of the target analyte. STA hydrogels show similar quenching values and time to steady state when compared to FF SWNT, but do not show a similar quenching rate to addition of the target analyte. The slower quenching rate of the STA gels could be due to incorporation of non-tethered SWNT sensors to the gel matrix.

Table 4-1: Quenching characteristics of hydrogel platforms. Fluorescence quenching is given in percentage of initial value and the time required for the fluorescence to reach a steady state value is given in seconds. The quenching rate is calculated from the quench value and the time required to reach steady state and is given in percentage quench per second. The quenching rate of the HALC platform was not significantly different from FF SWNT ($p>0.05$). The AC, ALC, and STA platforms had significantly different quenching rates from the FF SWNT ($p<0.05$), but the STA platform did not have a significantly different quench value or time to reach steady state from the FF SWNT ($p>0.05$). ($n = 3$).

| **Platform** | **Maximum Quenching Value [%]** | **Time to Steady State [s]** | **Quenching Rate [%/s]** |
|---|---|---|---|
| FF SWNT | 99.96 ± 0.04 | 9.87 ± 0.57 | 10.2 ± 0.557 |
| AC | 95.3 ± 2.66 | 551.2 ± 0.31 | 0.17 ± 0.005 |
| ALC | 80.16 ± 2.41 | 445.8 ± 39.97 | 0.18 ± 0.022 |
| HALC | 99.93 ± 0.07 | 10 ± 0.72 | 10.09 ± 0.7 |
| STA | 97.59 ± 0.17 | 20.53 ± 1.57 | 4.81 ± 0.392 |

We propose that the sensor quenching rate, and therefore maximum quench value within the 10-minute test period, is dependent on the SWNT's interaction with the hydrogel. The SWNT in the STA gels did not directly interact with the hydrogel, instead

there was a linker chain that bound the SWNT wrapping to the hydrogel. Similarly, a large volume of liquid within the core of the HALC gels allowed the majority of the SWNT to avoid physically interacting with the gel. The AC gel configuration allowed direct physical contact between the hydrogel material and the sensor, changing the ability of the sensor to interact with the analyte and therefore altering the sensor quenching rate. We hypothesized that the ALC gel was interacting with the sensor in a manner similar to that observed for the AC gel because of the small volume to surface area ratio of FF SWNT contained within the liquid core.

The importance of the volume to surface area ratio was tested with HALC gels, one with a large volume to surface ratio and the other with a small ratio. The previously described HALC gel is used for the high volume to surface ratio gel and a hyaluronic acid gel with two liquid cores (2HALC) is used for the small volume to surface ratio gel. By dividing the liquid core of the HALC gel a decrease in sensor volume occurs while increasing the surface area between the sensor and the gel. Testing of the HALC and 2HALC showed that the change in volume to surface area ratio significantly changed the fluorescence quenching rate (Figure 4-3b), with more interaction between the sensor and hydrogel leading to a slower quenching rate after the gels' exposure to an analyte solution.

These results show the ability to tune liquid core hydrogel sensor platforms. If a project requires real time feedback on analyte detection a large volume to surface area system can be utilized, but if a decreased number of readings to provide data about a larger span of time is preferred the volume to surface area ratio can be decreased.

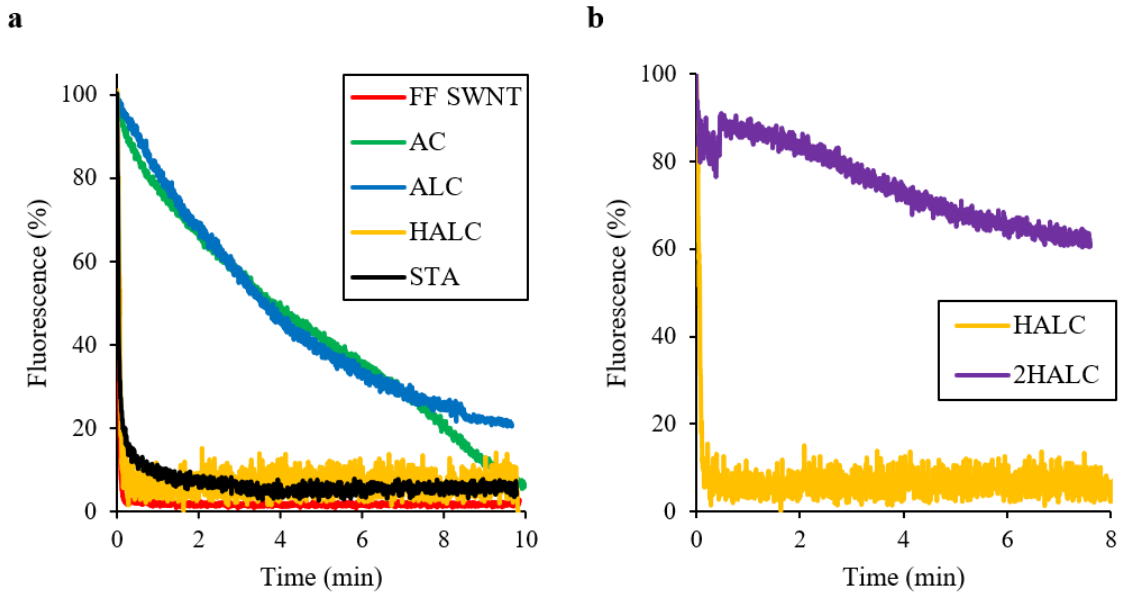


Figure 4-3: SWNT sensor response to analyte exposure is dependent on the hydrogel delivery platform. Quenching curves shown are the average of three trials (n = 3). a) ALC hydrogels showed delayed sensor response similar to what is observed for the AC gel. The STA and HALC hydrogels provide a stabilization platform to localize the SWNT while allowing free sensor interaction with the analyte, leading to sensor response similar to that observed in FF SWNT. b) 2HALC hydrogels had a significantly delayed sensor response compared to HALC indicating a response rate dependence on volume to surface area ratio of liquid core hydrogels.

### *4.4.4 Time to Sensor/Analyte Interaction*

Small analytes, such as NO, have very high diffusion rates.[176, 177] With the relatively large pore size, 5 nm for alginate and 5-12 nm for hyaluronic acid,[178, 179] of the hydrogels in comparison to NO it was hypothesized that NO would diffuse through the hydrogel quickly and the initial distance between the analyte and sensor would not be a rate determining factor in SWNT response. In order to quantify diffusion limitations for the hydrogel sensors, a second version of ALC hydrogel was made, one with a larger

hydrogel wall of 4 mm (thick ALC) than its counterpart with a wall of 2 mm (previously described ALC, which will be labeled thin ALC for this set of experiments). There was a significant difference in the SWNT quenching rate for the thin and thick ALC gels as shown in Figure 4-4a. Extrapolation of the quenching curves predicts that the thick ALC gel will take 66.3 minutes to reach steady state, whereas the thin ALC gel only took 7.5 minutes to reach steady state (Figure 4-4b) ($p<0.05$). The trend of gel thickness correlating to the time to reach steady state continues to hold true for the HALC gels, which similarly showed that a thicker hydrogel shell (2 mm, labeled thick HALC) took longer to quench than its thinner counterpart (previously described HALC gel which has a shell of 0.4 mm thickness, labeled thin HALC gel for this experiment) ($p<0.05$).

The comparison of the thick and thin hydrogels proves that sensors encapsulated within a hydrogel can have altered quenching rate due to the hydrogel alone, independent of the activity of the sensors. The change in time to reach steady state caused by hydrogel shell thickness provides another way to optimize a sensor platform to fit experimental needs.

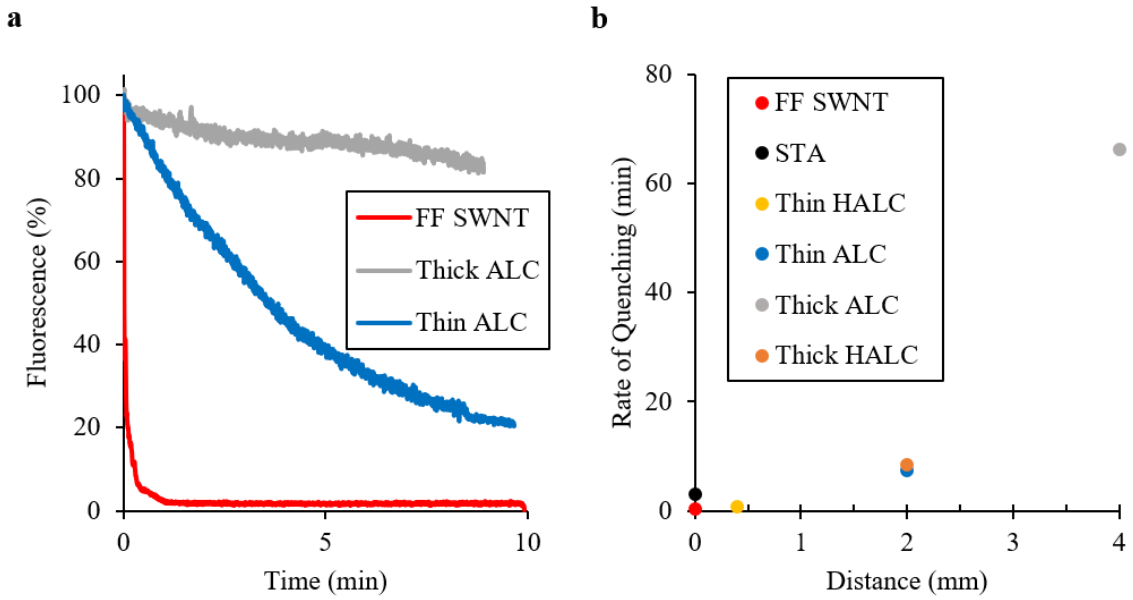


Figure 4-4: a) ALC hydrogels with either a thin or thick shell were exposed to the target analyte and the fluorescence was recorded. SWNT fluorescence quenching is shown to be significantly dependent on the distance between the sensor and the analyte solution. b) Hydrogel platforms that limit the distance from sensor to analyte display faster rates of signal quenching when compared to hydrogels that have a thicker shell between SWNT sensor solution and the surface of the gel ($p<0.05$). (n = 3, error bars are s.e.m)

### *4.4.5 Range of Response*

The importance of the sensor's freedom for movement and interactions was probed to see if physically constraining the SWNT changes its sensing characteristics. The STA hydrogel platform provides the opportunity to slightly alter the sensor's movement by altering the points of attachment between the sensor and the hydrogel surface. The average length of the SWNT sensors post sonication is ~150 nm,[49, 180, 181] with an average of 10 $(AT)_{15}$ strands wrapped around each nanotube.[150, 181-184]

By altering the $(AT)_{15}$ wrappings so that only a portion of the wrappings attach to the hydrogel surface a change in the sensor's freedom of movement can be achieved.
It was determined that altering the number of points of attachment between the sensor and hydrogel did not change the time to steady state, but it did alter the maximum quenching value. Three different compositions of STA gels were tested, one with all $(AT)_{15}$ wrappings attaching to the hydrogel (1:0 ratio of attached to non-attached), one with two thirds of the $(AT)_{15}$ wrappings attached to the hydrogel (2:1 ratio of attached to non-attached), and one with half of the $(AT)_{15}$ wrappings attached to the hydrogel (1:1 ratio of attached to non-attached, the previously discussed STA gels). The data shows that increasing the points of interaction between the sensor and the hydrogel surface decreases SWNT quenching (Figure 4-5a). It is hypothesized that constraining the sensor by having more points of attachment to the nanotube leads to the smaller quenching value. Decreasing the quenching value without increasing the microscope sensitivity results in a decrease in the sensitivity to changes in analyte concentration (Figure 4-5b). Therefore, increasing a sensor's range of movement leads to a more sensitive system. The quenching curve for the 2:1 STA hydrogel has more noise when compared to the other quenching curves. The three trials used to find the 2:1 STA average had more deviation and also did not provide as strong of a signal as the other STA hydrogels. When converting signal from a.u. to percentage the noise is amplified. The lower signal is due to a lower homogeneity in ssDNA wrapping distribution when compared to the 1:0 and 1:1 hydrogels.

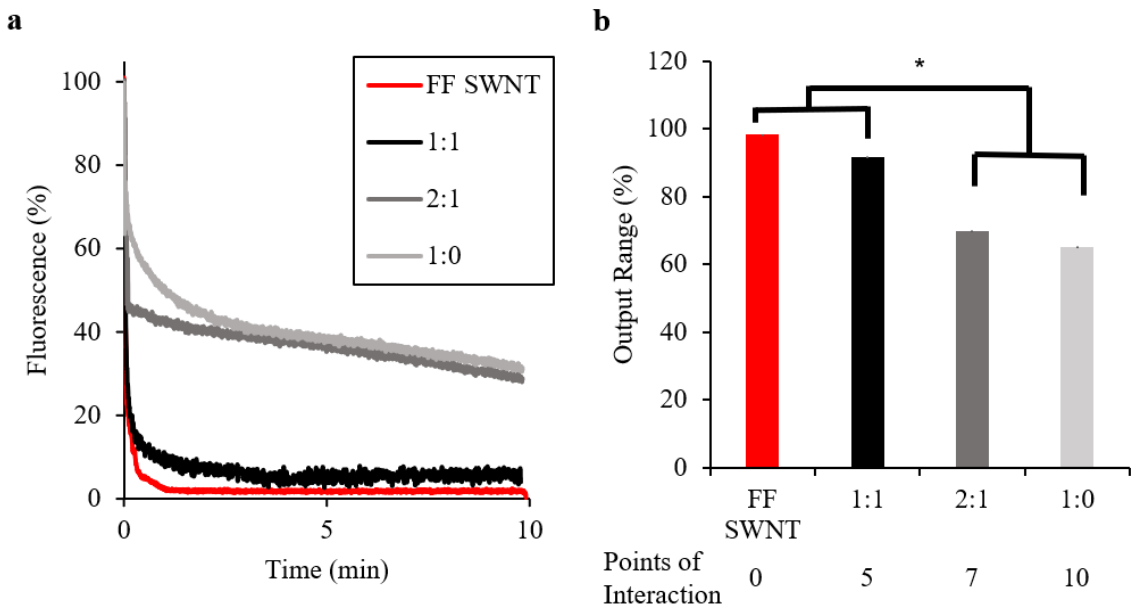


Figure 4-5: Surface-tethered hydrogels were modified with varying ratios of SWNT wrapping that interacted with the hydrogel to SWNT wrapping that did not interact with the hydrogel. a) The quenching rate was similar for the different ratios of SWNT wrapping that was attached to the hydrogel, but b) the output range was significantly altered by changing the number of interaction points between the sensor and the hydrogel, with more points of contact leading to significantly smaller output ranges ($p<0.05$) ($n = 3$, error bars are s.e.m).

## 4.5 Conclusions

Three novel hydrogel systems have been fabricated and characterized to improve sensitivity and reactivity of $(AT)_{15}$ wrapped SWNT sensors that are localized with an implantable platform. Utilizing the unique characteristics of the gels allowed for the determination of multiple ways to alter and optimize sensor platforms to fit specific requirements. The quenching rate for the liquid core sensors depends on their volume to surface area ratio and the thickness of the outer hydrogel shell. The alginate based liquid core system is hindered by a lack of even sensor distribution and reproducibility, but a

large number of gels can be quickly produced. The hyaluronic acid based liquid core system provides reproducible gels with an even distribution of the sensor, but the production of each gel requires a bit more time than its alginate counterpart.

While the surface tethered alginate gels consistently react at a fast rate to analyte exposure the range of sensing can be altered by changing the sensor's degrees of freedom. This alginate gel allows for the production of a large number of gels in a short amount of time while maintaining a fast reaction time similar to the free-floating sensors. Between the tunability of sensor response through alteration of the hydrogel platform and the long-term stability of all three of the new hydrogels described, multiple systems for *in vivo* sensing have been developed. The sensors used in this research react to nitric oxide, but SWNT can be used as sensors for a number of other analytes by changing its polymer wrapping.[185-187] It is possible to extend the use of the sensing platforms even farther by using other, non SWNT based sensors with these hydrogels.

The world of nanotechnology thrives on the development and use of small systems, but when a sensor needs to be stabilized *in vivo* going smaller is not always optimal. This research has shown three different sensor delivery platforms that allow nanoscale sensors to be utilized *in vivo* for extended periods of time without loss due to the migration of nanoscale systems.

## 4.6 Supplemental Information

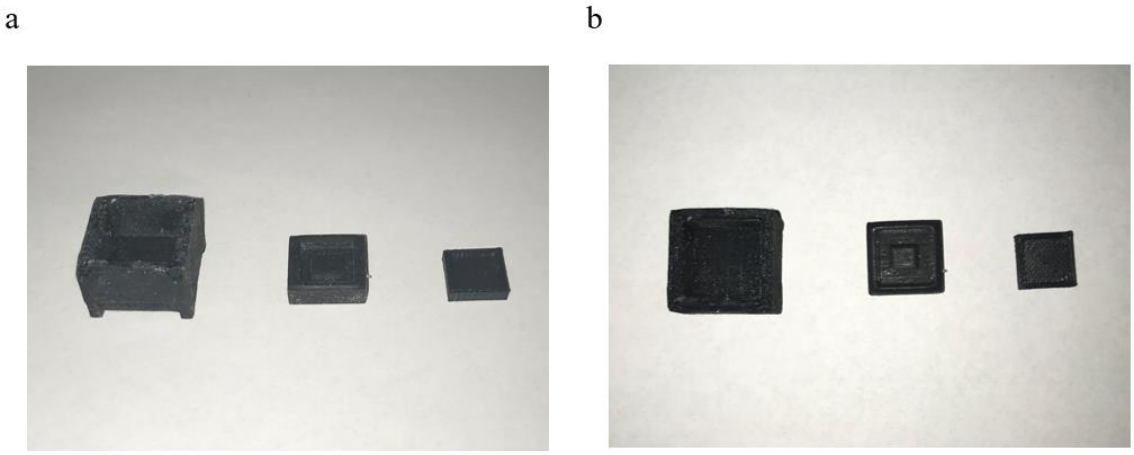


Figure 4-6: Molds used to create alginate liquid-core hydrogels from the (a) side and (b) top views. Smallest mold was used to create frozen core of SWNT sensor solution. Medium sized mold was used to create BaCl2 frozen halves to encase frozen SWNT sensor solution. Largest mold was used to hold alginate for crosslinking and allow addition of frozen BaCl2-SWNT sensor solution core.

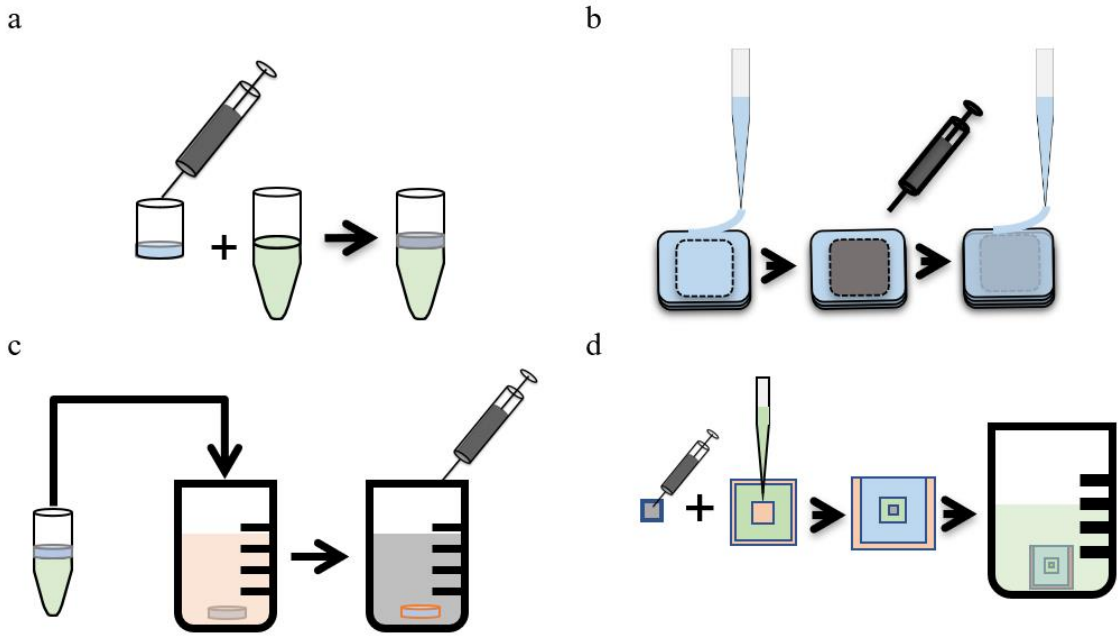


Figure 4-7: Schematic depicting various hydrogel fabrication methods. The black syringe represents the SWNT and where it was added to each hydrogel platform. (a) Alginate composite hydrogels were fabricated using mini dialysis membranes and suspending the SWNT sensors within alginate prior to crosslinking. (b) Hyaluronic acid liquid-core hydrogels were fabricated layer-by-layer using a 3D bioplotter and SWNT sensors were added during a pause in the printing process to the created voids in the hydrogel design prior to last layer deposition. (c) Surface-tethered alginate hydrogels were created stepwise by surface activation of alginate hydrogels with avidin and subsequent tethering of biotinylated SWNT sensors via SWNT bath. (d) Alginate liquid-core hydrogels were created using three molds, the first to freeze SWNT sensors creating a core, the second to surround SWNT core with frozen crosslinker, and the third to contain alginate for core addition and final crosslinking of hydrogel.

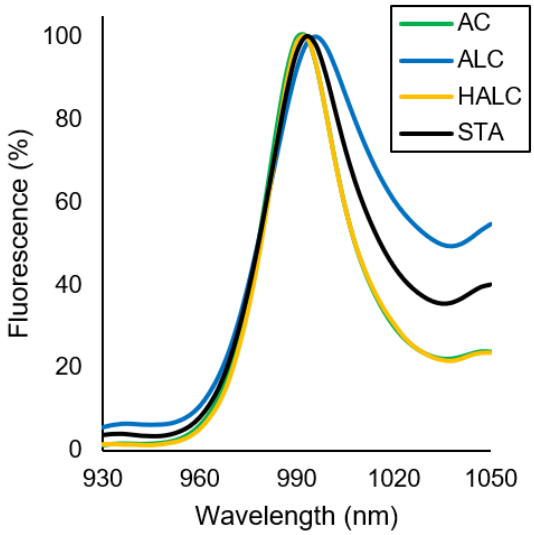


Figure 4-8: Sample spectra for each hydrogel platform type. Intensities were normalized to percentages of the maximum intensity value within each spectrum. Wavelength step size was 3 nm. A slight intensity shift (the peak is closer to the secondary peak) and red shift occur for ALC gels possibly due to increased imaging depth through the larger hydrogel shell for the intensity and a conformational change of the ssDNA on the SWNT for the red shift, however the SWNT sensors within this platform remain fluorescent and reactive to NO. The 990 nm peak is most prominent for the other gel platforms indicating 6,5 SWNT were successfully incorporated.

# CHAPTER 5

## Conclusions and Future Directions

### 5.1 Dissertation Conclusions

The work presented in this dissertation represents important steps in moving SWNT-based biosensors towards clinical translation. A biosensor needs to be biocompatible, easily detectable, and have a strong and rapid response to the target analyte in order to give providers access to valuable information on patient health and response to treatments for more personalized care and better outcomes.

Biocompatibility of SWNT has always been a concern due to the hydrophobic and persistent nature of the pure carbon structures. To mitigate these concerns, SWNT-hydrogel platforms were implanted *in vivo* and removed after two weeks. Novel extraction methods were developed to extract SWNT from the hydrogels and tissues of interest. Quantification using UV-Vis and Raman spectroscopy of the extracted nanotubes showed nearly 90% retention of the sensors by the hydrogels and no detectable SWNT in any of the tissues.

Large animal studies have remained elusive to the field of SWNT sensors due to difficulties associated with large animal housing and handling, and also because nanotechnology laboratories and detection setups are complex and nonportable. To this end, SWNT-hydrogel sensors were implanted into the ears of 14 male sheep, and, utilizing a newly developed portable, spectral imaging setup, assayed for signals. The new setup retained functionality of the more complex SWNT imaging systems that are commonly used, and the hydrogel platforms localized sensors without altering

responsiveness. Two thirds of the animals had distinguishable signals, demonstrating the first successful report of SWNT sensor signals in a large animal.

Most SWNT sensing applications rely on hydrogel platforms for localization *in vivo* due to the biocompatibility, mechanical properties, and optical transparency of most hydrogels. However, sensor response is greatly affected by incorporation into hydrogel matrices. In this work, analyte diffusion through the gel and the incorporation of the sensor were investigated and resulted in two novel hydrogel platforms that allowed SWNT to retain the fast detection rate of non-encapsulated SWNT while remaining localized to an implantable, biocompatible platform.

Together these results demonstrate SWNT as a biocompatible, easily detectable, and rapid *in vivo* biosensor. Extraction methods for quantifying SWNT sensors from hydrogels and tissues determines implanted SWNT's fate and mitigates toxicity concerns when using the sensors *in vivo*. Detection of SWNT signals in a large animal model demonstrates a relatively inexpensive and portable setup is capable of detecting a small volume of sensor away from the laboratory setting. Finally, the novel hydrogel platforms pave the road for better localization schemes for SWNT sensors by demonstrating the importance of platform design to optimize sensor performance. This work has helped move SWNT-based biosensors from the benchtop towards clinical translation, where application has the potential to revolutionize patient care by offering clinicians access to real-time, high resolution data of key biological markers and analytes to better personalize care and intervention.

## 5.2 Future Directions

### *5.2.1 Long-Term Fate of SWNT Sensors*

Although the biocompatibility study performed in this work was able to account for the vast majority of the initially implant SWNT sensors, alleviating toxicity concerns, leaching of sensors into the blood and tissues still could have occurred. A long-term study featuring collection of animal waste is needed in order to account for 100% of the sensors initially used in the study. Previous biodistribution work for SWNT sensors has shown a tendency for the nanotubes to aggregate in the filtering tissues, liver and kidney, for some time (days to weeks).[137, 188] Evidence points towards eventual clearing of the nanotubes in the waste; however, waste samples were not collected in this study due to logistical difficulties and concern of improper detection limits. Further development of nanotube extraction/quantification methods is required for an in depth, long-term fate determination of implanted SWNT sensors. One potential avenue of increased sensitivity would be hyperspectral fluorescence microscopy using high power nIR objectives. Single nanotube fluorescence is detectable using this kind of setup and would lead to the lowest possible detection limit for these nanoparticles.

### *5.2.2 Fixed Sensing Setup for Large Animals*

There is a need for a more stable and repeatable method of large animal fluorescence measurement. The animals in this study were difficult to handle and reacted

strongly to commotion associated with fluorescence readings using the spectrometer and light source on their ears. Sheep are also communicative herd animals, meaning the act of removing one sheep for measurement has effects on the remaining animals, causing stress and most likely elevated ROS and RNS, resulting in a fluorescence quenching of the NO sensors by the time the final animal was analyzed.[189] Experimenting with implant location may result in a more optimal location where the signal is still strong enough for detection and the animal is less disturbed by the measurement. One such location is on the hind leg near the tibia, where there is a thin stretched out portion of skin that would allow for light to excite the sensors and emission to pass through to the detector. Using the hind leg as an implant site would allow researchers to take measurements from the side or behind the animal, causing less commotion and stress, as sheep are prey animals with ~270° field of vision.[189] In addition, connection of the excitation liquid light guide to the spectrometer collimator via a U-shaped holder would allow for more rapid and precise measurements.

### *5.2.3 Hydrogel Tunability*

Although rapidly sensing SWNT-hydrogels were developed and were statistically similar to free floating sensors, hydrogel platforms can be expanded. Hydrogels offer many avenues of tunability including material, crosslinking density, and concentration.[172, 173, 179] Using rheological and mechanical testers, hydrogel stiffness could be tuned for the target tissue/application. Implants that do not effectively mimic native tissue tend to fail or cause the subject discomfort resulting in itching, which

will disrupt the primary function of many sensors as scratching causes inflammation, leading to overexpression of inflammatory agents in the area.[190]

Additionally, the hydrogel work discussed previously showed an ability to control sensor response to the target analyte either by manipulating the liquid core hydrogel thickness or by increasing or decreasing the points of interaction that the sensors had with the surface-tethered gel. The ability to control analyte/sensor interaction could be useful in designing a threshold sensing hydrogel platform, where only certain concentrations of analyte over a specific threshold cause fluorescence modulation either due to the diffusion gradient through the hydrogel wall or saturation of tightly bound surface sensors. In the case of nitric oxide, using an electrochemical probe and the NO sensing SWNT, the hydrogels could be made to only quench in the presence of a relatively large amount of NO, which would indicate an extraordinary biological event.

### *5.2.4 Sensor Patterning for Quantification*

Quantification of analytes has remained difficult for fluorescence-based sensors as modulations of the emission light can occur from the environment, nonspecific interactions, and overlapping signals.[191] There is a need for a sensing platform that would control the environment around the sensor while still allowing *in situ* detection of the target analyte. A patterned microfluidic device could be capable of fulfilling this need. SWNT sensors possess unparalleled spatiotemporal resolution, meaning they respond instantaneously to perturbations in their dielectric environment, and each individual nanotube acts as its own sensor. If the nanotubes could be incorporated into a

micropatterned device, the analyte of interest could be monitored in real time as it diffuses across the viewing window via SWNT fluorescence modulations. Using Fick's Law of Diffusion and known constants of the target analyte, concentration can be back calculated from the diffusion gradient.[192] Coupling such a patterned device with microfluidics would allow researchers to sample environmental conditions by flowing solution into the sensing platform for instantaneous concentration determination, then subsequently flushing the system for sensor recovery. In this manner, real time *in situ* sensors could be developed for any analyte in the SWNT sensor library, providing researchers an avenue of analyte detection and quantification for many situations and leading to a better understanding of biological pathways and disease progression/intervention.

## REFERENCES


1. Mehrotra, P., *Biosensors and their applications - A review.* Journal of oral biology and craniofacial research, 2016. **6**(2): p. 153-159.
2. Hillman, E.M.C., et al., *In vivo optical imaging and dynamic contrast methods for biomedical research.* Philosophical transactions. Series A, Mathematical, physical, and engineering sciences, 2011. **369**(1955): p. 4620-4643.
3. Cammann, K., *Bio-Senesors based on ion-selective electrodes.* Fresenius Journal of Analytical Chemistry, 1977. **287**: p. 1-9.
4. Wang, J., *Electrochemical Glucose Biosensors.* Chemical Reviews, 2008. **108**(2): p. 814-825.
5. Akyilmaz, E., E. Yorganci, and E. Asav, *Do copper ions activate tyrosinase enzyme? A biosensor model for the solution.* Bioelectrochemistry, 2010. **78**(2): p. 155-160.
6. Venugopal, V., *Biosensors in fish production and quality control.* Biosensors and Bioelectronics, 2002. **17**(3): p. 147-157.
7. Rechnitz, G., *Biochemical electrode uses tissue slices.* Chemical & Engineering News Archive, 1978. **56**(41): p. 16.
8. Wang, J., *DNA biosensors based on Peptide Nucleic Acid (PNA) recognition layers. A review1This paper was a finalist for the Biosensors & Bioelectronics Award for the most original contribution to the Congress.1.* Biosensors and Bioelectronics, 1998. **13**(7): p. 757-762.
9. Scognamiglio, V., et al., *Biosensing technology for sustainable food safety.* TrAC Trends in Analytical Chemistry, 2014. **62**: p. 1-10.
10. Leatherbarrow, R.J. and P.R. Edwards, *Analysis of molecular recognition using optical biosensors.* Current Opinion in Chemical Biology, 1999. **3**(5): p. 544-547.
11. He, X., et al., *Near-infrared fluorescent nanoprobes for cancer molecular imaging: status and challenges.* Trends in molecular medicine, 2010. **16**(12): p. 574-583.
12. Fan, X., et al., *Sensitive optical biosensors for unlabeled targets: A review.* analytica chimica acta, 2008. **620**(1-2): p. 8-26.
13. Liu, Y., X. Dong, and P. Chen, *Biological and chemical sensors based on graphene materials.* Chemical Society Reviews, 2012. **41**(6): p. 2283-2307.
14. Katz, E. and I. Willner, *Probing biomolecular interactions at conductive and semiconductive surfaces by impedance spectroscopy: routes to impedimetric immunosensors, DNA-sensors, and enzyme biosensors.* Electroanalysis: An International Journal Devoted to Fundamental and Practical Aspects of Electroanalysis, 2003. **15**(11): p. 913-947.
15. Jiang, P. and Z. Guo, *Fluorescent detection of zinc in biological systems: recent development on the design of chemosensors and biosensors.* Coordination chemistry reviews, 2004. **248**(1-2): p. 205-229.
16. Kuila, T., et al., *Recent advances in graphene-based biosensors.* Biosensors and bioelectronics, 2011. **26**(12): p. 4637-4648.

17. Heller, D.A., et al., *Multimodal optical sensing and analyte specificity using single-walled carbon nanotubes.* Nature Nanotechnology, 2009. **4**(2): p. 114.
18. Cai, Y., et al., *Optical nano-agents in the second near-infrared window for biomedical applications.* Chemical Society Reviews, 2019. **48**(1): p. 22-37.
19. Cooper, M.A., *Optical biosensors in drug discovery.* Nature reviews Drug discovery, 2002. **1**(7): p. 515.
20. Seydack, M., *Nanoparticle labels in immunosensing using optical detection methods.* Biosensors and bioelectronics, 2005. **20**(12): p. 2454-2469.
21. Diao, S., et al., *Chirality Enriched (12,1) and (11,3) Single-Walled Carbon Nanotubes for Biological Imaging.* Journal of the American Chemical Society, 2012. **134**(41): p. 16971-16974.
22. Yi, H., et al., *M13 phage-functionalized single-walled carbon nanotubes as nanoprobes for second near-infrared window fluorescence imaging of targeted tumors.* Nano letters, 2012. **12**(3): p. 1176-1183.
23. Welsher, K., S.P. Sherlock, and H. Dai, *Deep-tissue anatomical imaging of mice using carbon nanotube fluorophores in the second near-infrared window.* Proceedings of the National Academy of Sciences of the United States of America, 2011. **108**(22): p. 8943-8948.
24. Hong, G., et al., *Multifunctional in vivo vascular imaging using near-infrared II fluorescence.* Nature medicine, 2012. **18**(12): p. 1841-1846.
25. Robinson, J.T., et al., *In vivo fluorescence imaging in the second near-infrared window with long circulating carbon nanotubes capable of ultrahigh tumor uptake.* Journal of the American Chemical Society, 2012. **134**(25): p. 10664-10669.
26. CHANCE, B., *Near-Infrared Images Using Continuous, Phase-Modulated, and Pulsed Light with Quantitation of Blood and Blood Oxygenationa.* Annals of the New York Academy of Sciences, 1998. **838**(1): p. 29-45.
27. Anderson, R.R. and J.A. Parrish, *The Optics of Human Skin.* Journal of Investigative Dermatology, 1981. **77**(1): p. 13-19.
28. Smith, A.M., M.C. Mancini, and S. Nie, *Bioimaging: second window for in vivo imaging.* Nature nanotechnology, 2009. **4**(11): p. 710-711.
29. Zhang, H., et al., *Penetration depth of photons in biological tissues from hyperspectral imaging in shortwave infrared in transmission and reflection geometries.* Journal of biomedical optics, 2016. **21**(12): p. 126006-126006.
30. Chen, G., et al., *Nanochemistry and Nanomedicine for Nanoparticle-based Diagnostics and Therapy.* Chemical Reviews, 2016. **116**(5): p. 2826-2885.
31. Hemmer, E., et al., *Exploiting the biological windows: current perspectives on fluorescent bioprobes emitting above 1000 nm.* Nanoscale Horizons, 2016. **1**(3): p. 168-184.
32. Durduran, T., et al., *Diffuse Optics for Tissue Monitoring and Tomography.* Reports on progress in physics. Physical Society (Great Britain), 2010. **73**(7): p. 076701.
33. Zhang, J., et al., *Creating new fluorescent probes for cell biology.* Nature Reviews Molecular Cell Biology, 2002. **3**(12): p. 906-918.
34. Lippincott-Schwartz, J. and G.H. Patterson, *Development and Use of Fluorescent Protein Markers in Living Cells.* Science, 2003. **300**(5616): p. 87.

35. Shaner, N.C., P.A. Steinbach, and R.Y. Tsien, *A guide to choosing fluorescent proteins.* Nature Methods, 2005. **2**(12): p. 905-909.
36. Tsien, R.Y., *Building and breeding molecules to spy on cells and tumors.* FEBS Letters, 2005. **579**(4): p. 927-932.
37. Giepmans, B.N.G., et al., *The Fluorescent Toolbox for Assessing Protein Location and Function.* Science, 2006. **312**(5771): p. 217.
38. Ibraheem, A. and R.E. Campbell, *Designs and applications of fluorescent protein-based biosensors.* Current Opinion in Chemical Biology, 2010. **14**(1): p. 30-36.
39. Wu, B., et al., *Modern fluorescent proteins and imaging technologies to study gene expression, nuclear localization, and dynamics.* Current Opinion in Cell Biology, 2011. **23**(3): p. 310-317.
40. Aye-Han, N.-N., Q. Ni, and J. Zhang, *Fluorescent biosensors for real-time tracking of post-translational modification dynamics.* Current Opinion in Chemical Biology, 2009. **13**(4): p. 392-397.
41. Iijima, S., *Helical microtubules of graphitic carbon.* Nature, 1991. **354**(6348): p. 56-58.
42. Saito, R.D., G Dresselhaus, M S, *Physical Properties of Carbon Nanotubes*. Physical Properties of Carbon Nanotubes. 1998.
43. Zheng, M., *Sorting Carbon Nanotubes.* Top Curr Chem (Cham), 2017. **375**(1): p. 13.
44. Bachilo, S.M., et al., *Structure-Assigned Optical Spectra of Single-Walled Carbon Nanotubes.* Science, 2002. **298**(5602): p. 2361.
45. Hodge, S.A., et al., *Unweaving the rainbow: a review of the relationship between single-walled carbon nanotube molecular structures and their chemical reactivity.* Chemical Society Reviews, 2012. **41**(12): p. 4409-4429.
46. Naumov, A.V., et al., *Quantifying the Semiconducting Fraction in Single-Walled Carbon Nanotube Samples through Comparative Atomic Force and Photoluminescence Microscopies.* Nano Letters, 2009. **9**(9): p. 3203-3208.
47. Wilder, J.W.G., et al., *Electronic structure of atomically resolved carbon nanotubes.* Nature, 1998. **391**(6662): p. 59-62.
48. Kanemitsu, Y., *Excitons in semiconducting carbon nanotubes: diameter-dependent photoluminescence spectra.* Physical Chemistry Chemical Physics, 2011. **13**(33): p. 14879-14888.
49. O'Connell, M.J., et al., *Band Gap Fluorescence from Individual Single-Walled Carbon Nanotubes.* Science, 2002. **297**(5581): p. 593-596.
50. Jorio, A., et al., *Characterizing carbon nanotube samples with resonance Raman scattering.* New Journal of Physics, 2003. **5**: p. 139-139.
51. Kruss, S., et al., *Carbon nanotubes as optical biomedical sensors.* Advanced Drug Delivery Reviews, 2013. **65**(15): p. 1933-1950.
52. Liu, Z., et al., *Carbon nanotubes in biology and medicine: In vitro and in vivo detection, imaging and drug delivery.* Nano Research, 2009. **2**(2): p. 85-120.
53. Graff, R.A., et al., *Achieving individual-nanotube dispersion at high loading in single-walled carbon nanotube composites.* Advanced Materials, 2005. **17**(8): p. 980-984.
54. Kuzmany, H., et al., *Effect of dimensionality in polymeric fullerenes and single-wall nanotubes.* Physica B: Condensed Matter, 1998. **244**: p. 186-191.

55. Diao, S., et al., *Biological imaging without autofluorescence in the second near-infrared region.* Nano Research, 2015. **8**(9): p. 3027-3034.
56. Zhang, X. and Y. Pei, *Manipulation of charge transport in thermoelectrics.* npj Quantum Materials, 2017. **2**(1): p. 68.
57. Bahr, J.L. and J.M. Tour, *Covalent chemistry of single-wall carbon nanotubes.* Journal of Materials Chemistry, 2002. **12**(7): p. 1952-1958.
58. Zhang, J., et al., *Single molecule detection of nitric oxide enabled by d (AT) 15 DNA adsorbed to near infrared fluorescent single-walled carbon nanotubes.* Journal of the American Chemical Society, 2010. **133**(3): p. 567-581.
59. Kim, J.-H., et al., *The rational design of nitric oxide selectivity in single-walled carbon nanotube near-infrared fluorescence sensors for biological detection.* Nature Chemistry, 2009. **1**(6): p. 473.
60. Iverson, N.M., et al., *In vivo biosensing via tissue-localizable near-infrared-fluorescent single-walled carbon nanotubes.* Nat Nanotechnology, 2013. **8**(11): p. 873-80.
61. Ulissi, Z.W., et al., *Spatiotemporal intracellular nitric oxide signaling captured using internalized, near-infrared fluorescent carbon nanotube nanosensors.* Nano letters, 2014. **14**(8): p. 4887-4894.
62. Kruss, S., et al., *Neurotransmitter detection using corona phase molecular recognition on fluorescent single-walled carbon nanotube sensors.* Journal of the American Chemical Society, 2014. **136**(2): p. 713-724.
63. Harvey, J.D., et al., *Control of Carbon Nanotube Solvatochromic Response to Chemotherapeutic Agents.* ACS Applied Materials & Interfaces, 2017. **9**(43): p. 37947-37953.
64. Zubkovs, V., et al., *Mediatorless, Reversible Optical Nanosensor Enabled through Enzymatic Pocket Doping.* Small, 2017. **13**(42): p. 1701654.
65. Lee, K., J. Lee, and B. Ahn, *Design of Refolding DNA Aptamer on Single-Walled Carbon Nanotubes for Enhanced Optical Detection of Target Proteins.* Analytical Chemistry, 2019. **91**(20): p. 12704-12712.
66. Zhao, Y.-L. and J.F. Stoddart, *Noncovalent functionalization of single-walled carbon nanotubes.* Accounts of chemical research, 2009. **42**(8): p. 1161-1171.
67. Lew, T.T.S., et al., *Plant Nanobionic Sensors for Arsenic Detection.* Advanced Materials, 2021. **33**(1): p. 2005683.
68. Satishkumar, B., et al., *Reversible fluorescence quenching in carbon nanotubes for biomolecular sensing.* Nature Nanotechnology, 2007. **2**(9): p. 560.
69. Beyene, A.G., et al., *Imaging striatal dopamine release using a nongenetically encoded near infrared fluorescent catecholamine nanosensor.* Science advances, 2019. **5**(7): p. eaaw3108.
70. Welsher, K., et al., *Selective probing and imaging of cells with single walled carbon nanotubes as near-infrared fluorescent molecules.* Nano letters, 2008. **8**(2): p. 586-590.
71. Heller, D.A., et al., *Optical detection of DNA conformational polymorphism on single-walled carbon nanotubes.* Science, 2006. **311**(5760): p. 508-511.
72. Jeng, E.S., et al., *Detection of DNA hybridization using the near-infrared band-gap fluorescence of single-walled carbon nanotubes.* Nano letters, 2006. **6**(3): p. 371-375.

73. Kruss, S., et al., *High-resolution imaging of cellular dopamine efflux using a fluorescent nanosensor array.* Proceedings of the National Academy of Sciences, 2017. **114**(8): p. 1789-1794.
74. Harvey, J.D., et al., *An in Vivo Nanosensor Measures Compartmental Doxorubicin Exposure.* Nano Letters, 2019. **19**(7): p. 4343-4354.
75. Zhang, J., et al., *Molecular recognition using nanotube-adsorbed polymer phases: nanotube antibodies.* Nature nanotechnology, 2013. **8**(12): p. 959.
76. Barone, P.W., et al., *Near-infrared optical sensors based on single-walled carbon nanotubes.* Nature materials, 2005. **4**(1): p. 86.
77. Williams, R.M., et al., *Glutathione-S-transferase Fusion Protein Nanosensor.* Nano Letters, 2020. **20**(10): p. 7287-7295.
78. Harvey, J.D., et al., *HIV Detection via a Carbon Nanotube RNA Sensor.* ACS Sensors, 2019. **4**(5): p. 1236-1244.
79. Landry, M.P., et al., *Single-molecule detection of protein efflux from microorganisms using fluorescent single-walled carbon nanotube sensor arrays.* Nature nanotechnology, 2017. **12**(4): p. 368-377.
80. Dong, J., et al., *Analysis of Multiplexed Nanosensor Arrays Based on Near-Infrared Fluorescent Single-Walled Carbon Nanotubes.* ACS Nano, 2018. **12**(4): p. 3769-3779.
81. Jin, H., et al., *Detection of single-molecule H 2 O 2 signalling from epidermal growth factor receptor using fluorescent single-walled carbon nanotubes.* Nature Nanotechnology, 2010. **5**(4): p. 302.
82. Kim, J.-H., et al., *Single-molecule detection of H2O2 mediating angiogenic redox signaling on fluorescent single-walled carbon nanotube array.* Acs Nano, 2011. **5**(10): p. 7848-7857.
83. Bisker, G., et al., *Insulin Detection Using a Corona Phase Molecular Recognition Site on Single-Walled Carbon Nanotubes.* ACS Sensors, 2018. **3**(2): p. 367-377.
84. Galassi, T.V., et al., *An optical nanoreporter of endolysosomal lipid accumulation reveals enduring effects of diet on hepatic macrophages in vivo.* Science Translational Medicine, 2018. **10**(461): p. eaar2680.
85. Chio, L., et al., *Electrostatic Assemblies of Single-Walled Carbon Nanotubes and Sequence-Tunable Peptoid Polymers Detect a Lectin Protein and Its Target Sugars.* Nano Letters, 2019.
86. Jena, P.V., et al., *A carbon nanotube optical reporter maps endolysosomal lipid flux.* ACS nano, 2017. **11**(11): p. 10689-10703.
87. Harvey, J.D., et al., *A carbon nanotube reporter of microRNA hybridization events in vivo.* Nature biomedical engineering, 2017. **1**(4): p. 0041.
88. Budhathoki-Uprety, J., et al., *Synthetic molecular recognition nanosensor paint for microalbuminuria.* Nature communications, 2019. **10**(1): p. 1-9.
89. Lee, M.A., et al., *Implantable Nanosensors for Human Steroid Hormone Sensing In Vivo Using a Self-Templating Corona Phase Molecular Recognition.* Advanced Healthcare Materials, 2020. **9**(21): p. 2000429.
90. Lee, M.A., et al., *Implanted Nanosensors in Marine Organisms for Physiological Biologging: Design, Feasibility, and Species Variability.* ACS sensors, 2018. **4**(1): p. 32-43.

91. Pinals, R.L., et al., *Rapid SARS-CoV-2 Spike Protein Detection by Carbon Nanotube-Based Near-Infrared Nanosensors.* Nano Letters, 2021. **21**(5): p. 2272-2280.
92. Jeong, S., et al., *High Throughput Evolution of Near Infrared Serotonin Nanosensors.* bioRxiv, 2019: p. 673152.
93. Jeng, E.S., et al., *Detection of a Single Nucleotide Polymorphism Using Single-Walled Carbon-Nanotube Near-Infrared Fluorescence.* Small, 2010. **6**(1): p. 40-43.
94. Zhang, J., et al., *A rapid, direct, quantitative, and label-free detector of cardiac biomarker troponin T using near-infrared fluorescent single-walled carbon nanotube sensors.* Advanced healthcare materials, 2014. **3**(3): p. 412-423.
95. Yaari, Z., et al., *Nanoreporter of an Enzymatic Suicide Inactivation Pathway.* Nano Letters, 2020. **20**(11): p. 7819-7827.
96. Dong, J., et al., *A synthetic mimic of phosphodiesterase type 5 based on corona phase molecular recognition of single-walled carbon nanotubes.* Proceedings of the National Academy of Sciences, 2020. **117**(43): p. 26616.
97. Dinarvand, M., et al., *Near-Infrared Imaging of Serotonin Release from Cells with Fluorescent Nanosensors.* Nano Letters, 2019. **19**(9): p. 6604-6611.
98. Budhathoki-Uprety, J., et al., *A Carbon Nanotube Optical Sensor Reports Nuclear Entry via a Noncanonical Pathway.* ACS Nano, 2017. **11**(4): p. 3875-3882.
99. Williams, R.M., C. Lee, and D.A. Heller, *A Fluorescent Carbon Nanotube Sensor Detects the Metastatic Prostate Cancer Biomarker uPA.* ACS Sensors, 2018. **3**(9): p. 1838-1845.
100. Williams, R.M., et al., *Noninvasive ovarian cancer biomarker detection via an optical nanosensor implant.* Science Advances, 2018. **4**(4): p. eaaq1090.
101. Lin, C.-W., et al., *In vivo optical detection and spectral triangulation of carbon nanotubes.* ACS applied materials & interfaces, 2017. **9**(48): p. 41680-41690.
102. Bonis-O'Donnell, J.T.D., et al., *Dual Near-Infrared Two-Photon Microscopy for Deep-Tissue Dopamine Nanosensor Imaging.* Advanced Functional Materials, 2017. **27**(39): p. 1702112.
103. Hansen, S.F. and A. Lennquist, *Carbon nanotubes added to the SIN List as a nanomaterial of Very High Concern.* Nature Nanotechnology, 2020. **15**(1): p. 3-4.
104. Lam, C.-W., et al., *Pulmonary Toxicity of Single-Wall Carbon Nanotubes in Mice 7 and 90 Days After Intratracheal Instillation.* Toxicological Sciences, 2004. **77**(1): p. 126-134.
105. Poland, C.A., et al., *Carbon nanotubes introduced into the abdominal cavity of mice show asbestos-like pathogenicity in a pilot study.* Nature Nanotechnology, 2008. **3**(7): p. 423-428.
106. Ali-Boucetta, H., et al., *Asbestos-like Pathogenicity of Long Carbon Nanotubes Alleviated by Chemical Functionalization.* Angewandte Chemie International Edition, 2013. **52**(8): p. 2274-2278.
107. Movia, D., et al., *Screening the Cytotoxicity of Single-Walled Carbon Nanotubes Using Novel 3D Tissue-Mimetic Models.* ACS Nano, 2011. **5**(11): p. 9278-9290.
108. Ema, M., M. Gamo, and K. Honda, *A review of toxicity studies of single-walled carbon nanotubes in laboratory animals.* Regulatory Toxicology and Pharmacology, 2016. **74**: p. 42-63.

109. Kermanizadeh, A., et al., *A Multilaboratory Toxicological Assessment of a Panel of 10 Engineered Nanomaterials to Human Health—ENPRA Project—The Highlights, Limitations, and Current and Future Challenges.* Journal of Toxicology and Environmental Health, Part B, 2016. **19**(1): p. 1-28.
110. Kostarelos, K., *The long and short of carbon nanotube toxicity.* Nature Biotechnology, 2008. **26**(7): p. 774-776.
111. Castagnola, V., et al., *Towards a classification strategy for complex nanostructures.* Nanoscale Horizons, 2017. **2**(4): p. 187-198.
112. Iverson, N.M., et al., *In vivo biosensing via tissue-localizable near-infrared-fluorescent single-walled carbon nanotubes.* Nature nanotechnology, 2013. **8**(11): p. 873.
113. Heller, D.A., et al., *Banning carbon nanotubes would be scientifically unjustified and damaging to innovation.* Nature Nanotechnology, 2020. **15**(3): p. 164-166.
114. Alidori, S., et al., *Carbon nanotubes exhibit fibrillar pharmacology in primates.* PLOS ONE, 2017. **12**(8): p. e0183902.
115. Galassi, T.V., et al., *Long-term in vivo biocompatibility of single-walled carbon nanotubes.* PloS one, 2020. **15**(5): p. e0226791-e0226791.
116. Scheerlinck, J.-P.Y., et al., *Biomedical applications of sheep models: from asthma to vaccines.* Trends in Biotechnology, 2008. **26**(5): p. 259-266.
117. Mestas, J. and C.C. Hughes, *Of mice and not men: differences between mouse and human immunology.* J Immunol, 2004. **172**(5): p. 2731-8.
118. Rong, G., S.R. Corrie, and H.A. Clark, *In Vivo Biosensing: Progress and Perspectives.* ACS sensors, 2017. **2**(3): p. 327-338.
119. Leeuw, T.K., et al., *Single-walled carbon nanotubes in the intact organism: near-IR imaging and biocompatibility studies in Drosophila.* Nano letters, 2007. **7**(9): p. 2650-2654.
120. Iverson, N.M., et al., *Quantitative Tissue Spectroscopy of Near Infrared Fluorescent Nanosensor Implants.* Journal of Biomedical Nanotechnology, 2016. **12**(5): p. 1035-1047.
121. Chang, A.-Y., et al., *Dopamine sensing with robust carbon nanotube implanted polymer micropillar array electrodes fabricated by coupling micromolding and infiltration coating processes.* Electrochimica Acta, 2021. **368**: p. 137632.
122. Streit, J.K., et al., *Measuring single-walled carbon nanotube length distributions from diffusional trajectories.* Acs Nano, 2012. **6**(9): p. 8424-8431.
123. Nanot, S., et al., *Single-Walled Carbon Nanotubes*, in *Springer Handbook of Nanomaterials*. 2013, Springer. p. 105-146.
124. Zhu, H., et al., *Direct synthesis of long single-walled carbon nanotube strands.* Science, 2002. **296**(5569): p. 884-886.
125. Zheng, L., et al., *Ultralong single-wall carbon nanotubes.* Nature materials, 2004. **3**(10): p. 673.
126. O'connell, M.J., et al., *Band gap fluorescence from individual single-walled carbon nanotubes.* Science, 2002. **297**(5581): p. 593-596.
127. Strano, M.S., et al., *Electronic structure control of single-walled carbon nanotube functionalization.* Science, 2003. **301**(5639): p. 1519-1522.
128. Dresselhaus, G. and S. Riichiro, *Physical properties of carbon nanotubes*. 1998: World scientific.

129. Kim, B.C., et al., *Fabrication of enzyme-based coatings on intact multi-walled carbon nanotubes as highly effective electrodes in biofuel cells.* Scientific reports, 2017. **7**: p. 40202.
130. Strano, M.S., et al., *The role of surfactant adsorption during ultrasonication in the dispersion of single-walled carbon nanotubes.* Journal of nanoscience and nanotechnology, 2003. **3**(1-2): p. 81-86.
131. Barone, P.W., R.S. Parker, and M.S. Strano, *In vivo fluorescence detection of glucose using a single-walled carbon nanotube optical sensor: design, fluorophore properties, advantages, and disadvantages.* Analytical chemistry, 2005. **77**(23): p. 7556-7562.
132. Moore, V.C., et al., *Individually suspended single-walled carbon nanotubes in various surfactants.* Nano letters, 2003. **3**(10): p. 1379-1382.
133. Zheng, M., et al., *DNA-assisted dispersion and separation of carbon nanotubes.* Nature materials, 2003. **2**(5): p. 338.
134. Heller, D.A., et al., *Single-Walled Carbon Nanotube Spectroscopy in Live Cells: Towards Long-Term Labels and Optical Sensors.* Advanced Materials, 2005. **17**(23): p. 2793-2799.
135. Mann, F.A., et al., *Tuning Selectivity of Fluorescent Carbon Nanotube-Based Neurotransmitter Sensors.* Sensors (Basel, Switzerland), 2017. **17**(7): p. 1521.
136. Mann, F.A., et al., *Nanobody-Conjugated Nanotubes for Targeted Near-Infrared In Vivo Imaging and Sensing.* Angewandte Chemie International Edition, 2019. **58**(33): p. 11469-11473.
137. Liu, Z., et al., *Circulation and long-term fate of functionalized, biocompatible single-walled carbon nanotubes in mice probed by Raman spectroscopy.* Proceedings of the National Academy of Sciences, 2008. **105**(5): p. 1410.
138. Galassi, T.V., et al., *An optical nanoreporter of endolysosomal lipid accumulation reveals enduring effects of diet on hepatic macrophages in vivo.* Science translational medicine, 2018. **10**(461): p. eaar2680.
139. Greenberg, S.S., D.E. Wilcox, and G.M. Rubanyi, *Endothelium-derived relaxing factor released from canine femoral artery by acetylcholine cannot be identified as free nitric oxide by electron paramagnetic resonance spectroscopy.* Circulation research, 1990. **67**(6): p. 1446-1452.
140. Brown, J., et al., *Nitric oxide generators and cGMP stimulate mucus secretion by rat gastric mucosal cells.* American Journal of Physiology-Gastrointestinal and Liver Physiology, 1993. **265**(3): p. G418-G422.
141. Cui, S., et al., *Activated murine macrophages induce apoptosis in tumor cells through nitric oxide-dependent or-independent mechanisms.* Cancer Research, 1994. **54**(9): p. 2462-2467.
142. Contestabile, A. and E. Ciani, *Role of nitric oxide in the regulation of neuronal proliferation, survival and differentiation.* Neurochemistry international, 2004. **45**(6): p. 903-914.
143. Arroyo, C.M. and M. Kohno, *Difficulties encountered in the detection of nitric oxide (NO) by spin trapping techniques. A cautionary note.* Free radical research communications, 1991. **14**(2): p. 145-155.
144. Iverson, N., E. Hofferber, and J. Stapleton, *Nitric Oxide Sensors for Biological Applications.* Chemosensors, 2018. **6**(1): p. 8.

145. Hofferber, E.M., et al., *Implantable Nanotube Sensor Platform for Rapid Analyte Detection.* Macromolecular Bioscience, 2019. **19**(6): p. 1800469.
146. Bhalla, N., et al., *Opportunities and Challenges for Biosensors and Nanoscale Analytical Tools for Pandemics: COVID-19.* ACS Nano, 2020. **14**(7): p. 7783-7807.
147. Shumeiko, V., et al., *A Paper-Based Near-Infrared Optical Biosensor for Quantitative Detection of Protease Activity Using Peptide-Encapsulated SWCNTs.* Sensors, 2020. **20**(18).
148. Pinals, R.L., et al., *Corona Exchange Dynamics on Carbon Nanotubes by Multiplexed Fluorescence Monitoring.* Journal of the American Chemical Society, 2020. **142**(3): p. 1254-1264.
149. Nißler, R., et al., *Quantification of the Number of Adsorbed DNA Molecules on Single-Walled Carbon Nanotubes.* The Journal of Physical Chemistry C, 2019. **123**(8): p. 4837-4847.
150. Zhang, J., et al., *Single Molecule Detection of Nitric Oxide Enabled by d(AT)15 DNA Adsorbed to Near Infrared Fluorescent Single-Walled Carbon Nanotubes.* Journal of the American Chemical Society, 2011. **133**(3): p. 567-581.
151. Pinals, R.L., et al., *Rapid SARS-CoV-2 Detection by Carbon Nanotube-Based Near-Infrared Nanosensors.* medRxiv, 2020: p. 2020.11.02.20223404.
152. Hofferber, E., et al., *Novel Methods to Extract and Quantify Sensors based on Single Wall Carbon Nanotube Fluorescence from Animal Tissue and Hydrogel-Based Platforms.* Methods and Applications in Fluorescence, 2021.
153. Iverson, N.M., et al., *In vivo biosensing via tissue-localizable near-infrared-fluorescent single-walled carbon nanotubes.* Nature Nanotechnology, 2013. **8**: p. 873.
154. Wray, S., et al., *Characterization of the near infrared absorption spectra of cytochrome aa3 and haemoglobin for the non-invasive monitoring of cerebral oxygenation.* Biochimica et Biophysica Acta (BBA) - Bioenergetics, 1988. **933**(1): p. 184-192.
155. Wu, W., et al., *Targeted delivery of amphotericin B to cells by using functionalized carbon nanotubes.* Angew Chem Int Ed Engl, 2005. **44**(39): p. 6358-62.
156. Kam, N.W.S., et al., *Carbon nanotubes as multifunctional biological transporters and near-infrared agents for selective cancer cell destruction.* Proceedings of the National Academy of Sciences of the United States of America, 2005. **102**(33): p. 11600-11605.
157. Iverson, N.M., et al., *In vivo biosensing via tissue-localizable near-infrared-fluorescent single-walled carbon nanotubes.* Nature Nanotechnology, 2013. **8**(11): p. 873-880.
158. Liu, Z., et al., *Supramolecular Chemistry on Water-Soluble Carbon Nanotubes for Drug Loading and Delivery.* ACS Nano, 2007. **1**(1): p. 50-56.
159. Dumortier, H., et al., *Functionalized carbon nanotubes are non-cytotoxic and preserve the functionality of primary immune cells.* Nano Lett, 2006. **6**(7): p. 1522-8.
160. Chen, X., et al., *Interfacing Carbon Nanotubes with Living Cells.* Journal of the American Chemical Society, 2006. **128**(19): p. 6292-6293.

161. Chin, S.F., et al., *Amphiphilic helical peptide enhances the uptake of single-walled carbon nanotubes by living cells.* Exper. Biol. Med., 2007. **232**: p. 1236-1244.
162. Yehia, H.N., et al., *Single-walled carbon nanotube interactions with HeLa cells.* J Nanobiotechnology, 2007. **5**: p. 8.
163. Schipper, M.L., et al., *A pilot toxicology study of single-walled carbon nanotubes in a small sample of mice.* Nature nanotechnology, 2008. **3**(4): p. 216-221.
164. Cherukuri, P., et al., *Near-infrared fluorescence microscopy of single-walled carbon nanotubes in phagocytic cells.* Journal of the American Chemical Society, 2004. **126**(48): p. 15638–15639.
165. Iverson, N., et al., *Quantitative Tissue Spectroscopy of Near Infrared Fluorescent Nanosensor Implants.* Journal of Biomedical Nanotechnology, 2016. **12**(5): p. 1035-1047.
166. Cho, W.J., S.H. Oh, and J.H. Lee, *Alginate Film as a Novel Post-Surgical Tissue Adhesion Barrier.* Journal of Biomaterials Science, Polymer Edition, 2010. **21**(6-7): p. 701-713.
167. Lee, K.Y. and D.J. Mooney, *Alginate: properties and biomedical applications.* Progress in polymer science, 2012. **37**(1): p. 106-126.
168. Ulery, B.D., L.S. Nair, and C.T. Laurencin, *Biomedical Applications of Biodegradable Polymers.* Journal of polymer science. Part B, Polymer physics, 2011. **49**(12): p. 832-864.
169. Sultzbaugh, K.J. and T.J. Speaker, *A method to attach lectins to the surface of spermine alginate microcapsules based on the avidin biotin interaction.* J Microencapsul, 1996. **13**(4): p. 363-76.
170. Roxbury, D., et al., *Hyperspectral Microscopy of Near-Infrared Fluorescence Enables 17-Chirality Carbon Nanotube Imaging.* Scientific Reports, 2015. **5**: p. 14167.
171. Tam, S.K., et al., *Factors influencing alginate gel biocompatibility.* Journal of Biomedical Materials Research Part A, 2011. **98A**(1): p. 40-52.
172. Lee, K.Y., et al., *Controlling Mechanical and Swelling Properties of Alginate Hydrogels Independently by Cross-Linker Type and Cross-Linking Density.* Macromolecules, 2000. **33**(11): p. 4291-4294.
173. Matyash, M., et al., *Swelling and Mechanical Properties of Alginate Hydrogels with Respect to Promotion of Neural Growth.* Tissue Engineering Part C: Methods, 2013. **20**(5): p. 401-411.
174. Attal, S., R. Thiruvengadathan, and O. Regev, *Determination of the Concentration of Single-Walled Carbon Nanotubes in Aqueous Dispersions Using UV−Visible Absorption Spectroscopy.* Analytical Chemistry, 2006. **78**(23): p. 8098-8104.
175. Kim, J.-H., et al., *The rational design of nitric oxide selectivity in single-walled carbon nanotube near-infrared fluorescence sensors for biological detection.* Nature Chemistry, 2009. **1**: p. 473.
176. Zacharia, I.G. and W.M. Deen, *Diffusivity and Solubility of Nitric Oxide in Water and Saline.* Annals of Biomedical Engineering, 2005. **33**(2): p. 214-222.

177. Beckman, J.S. and W.H. Koppenol, *Nitric oxide, superoxide, and peroxynitrite: the good, the bad, and ugly.* American Journal of Physiology-Cell Physiology, 1996. **271**(5): p. C1424-C1437.
178. Boontheekul, T., H.-J. Kong, and D.J. Mooney, *Controlling alginate gel degradation utilizing partial oxidation and bimodal molecular weight distribution.* Biomaterials, 2005. **26**(15): p. 2455-2465.
179. Xu, X., et al., *Hyaluronic Acid-Based Hydrogels: from a Natural Polysaccharide to Complex Networks.* Soft matter, 2012. **8**(12): p. 3280-3294.
180. Nakayama-Ratchford, N., et al., *Non-Covalent Functionalization of Carbon Nanotubes by Fluorescein-Polyethylene Glycol: Supramolecular Conjugates with pH Dependent Absorbance and Fluorescence.* Journal of the American Chemical Society, 2007. **129**(9): p. 2448-2449.
181. Zheng, M., et al., *Structure-Based Carbon Nanotube Sorting by Sequence-Dependent DNA Assembly.* Science, 2003. **302**(5650): p. 1545.
182. Jin, H., et al., *Divalent Ion and Thermally Induced DNA Conformational Polymorphism on Single-walled Carbon Nanotubes.* Macromolecules, 2007. **40**(18): p. 6731-6739.
183. Campbell, J.F., et al., *Atomic Force Microscopy Studies of DNA-Wrapped Carbon Nanotube Structure and Binding to Quantum Dots.* Journal of the American Chemical Society, 2008. **130**(32): p. 10648-10655.
184. Harvey, J.D., et al., *A Carbon Nanotube Reporter of miRNA Hybridization Events In Vivo.* Nature biomedical engineering, 2017. **1**: p. 0041.
185. Heller, D.A., et al., *Multimodal optical sensing and analyte specificity using single-walled carbon nanotubes.* Nature Nanotechnology, 2008. **4**: p. 114.
186. Barone, P.W., et al., *Near-infrared optical sensors based on single-walled carbon nanotubes.* Nature Materials, 2005. **4**(1): p. 86-U16.
187. Landry, M.P., et al., *Experimental tools to study molecular recognition within the nanoparticle corona.* Sensors, 2014. **14**(9): p. 16196-16211.
188. Jena, P.V., et al., *Progress toward Applications of Carbon Nanotube Photoluminescence.* ECS Journal of Solid State Science and Technology, 2017. **6**(6): p. M3075-M3077.
189. Marino, L. and D.L. Merskin. *Intelligence, complexity, and individuality in sheep*. 2019.
190. Abraham, A.A., et al., *Foreign Body Reaction to a Subcutaneously Implanted Self-Cleaning, Thermoresponsive Hydrogel Membrane for Glucose Biosensors.* ACS biomaterials science & engineering, 2018. **4**(12): p. 4104-4111.
191. Park, S.-H., et al., *Synthetic ratiometric fluorescent probes for detection of ions.* Chemical Society Reviews, 2020. **49**(1): p. 143-179.
192. Saunders, J.E., et al., *Quantitative diffusion and swelling kinetic measurements using large-angle interferometric refractometry.* Soft Matter, 2015. **11**(45): p. 8746-8757.